AD NUMBER

ADB015176

LIMITATION CHANGES

TO:

Approved for public release; distribution is unlimited.

FROM:

Distribution authorized to U.S. Gov't. agencies only; Test and Evaluation; OCT 1975. Other requests shall be referred to Air Force Avionics Lab., Wright-Patterson AFB, OH 45433.

AUTHORITY

AFAL ltr 7 May 1979

AFAL-TR-75-191

SOLAR PUMPED LASER

GTE SYLVANIA, INC.
ELECTRO-OPTICS ORGANIZATION ,
POST OFFICE BOX 188
MOUNTAIN VIEW, CALIFORNIA 94042

SEPTEMBER 1976

TECHNICAL REPORT AFAL-TR-75-191
FINAL REPORT FOR PERIOD 18 FEBRUARY 1974 - 11 JULY 1975

AIR FORCE AVIONICS LABORATORY
AIR FORCE WRIGHT AERONAUTICAL LABORATORIES
AIR FORCE SYSTEMS COMMAND
WRIGHT-PATTERSON AIR FORCE BASE, OHIO 45433

NOTICE

When Government drawings, specifications, or other data are used for any purpose other than in connection with a definitely related Government procurement operation, the United States Government thereby incurs no responsibility nor any obligation whatsoever; and the fact that the government may have formulated, furnished, or in any way supplied the said drawings, specifications, or other data, is not to be regarded by implication or otherwise as in any manner licensing the holder or any other person or corporation, or conveying any rights or permission to manufacture, use, or sell any patented invention that may in any way be related thereto.

This technical report has been reviewed and is approved for publication.

Donald D. Matulka
Donald D. Matulka
Project Engineer
Electro-Optic Detectors Group
Electro-Optics Technology Branch

Donald J. Peacock
DONALD J. PEACOCK, Actg. Chief
Electro-Optic Detectors Group
Electro-Optics Technology Branch

FOR THE COMMANDER

William C. Schoonover
WILLIAM C. SCHOONOVER, Chief
Electro-Optics Technology Branch
Electronic Technology Division

Copies of this report should not be returned unless return is required by security considerations, contractual obligations, or notice on a specific document.

AIR FORCE - 29 OCTOBER 76 - 100

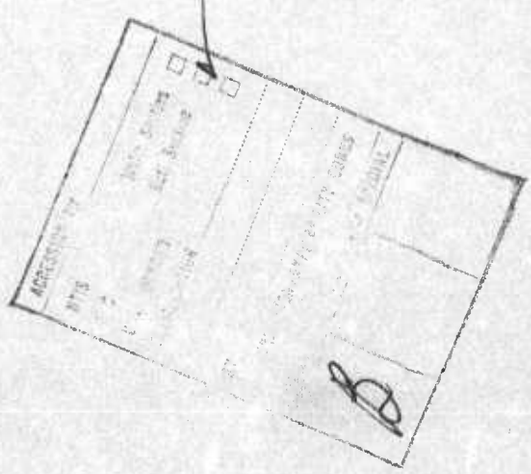

UNCLASSIFIED

SECURITY CLASSIFICATION OF THIS PAGE (When Data Entered)

REPORT DOCUMENTATION PAGE

READ INSTRUCTIONS BEFORE COMPLETING FORM

1. REPORT NUMBER: AFAL-TR-75-191	2. GOVT ACCESSION NO.
3. RECIPIENT'S CATALOG NUMBER	
4. TITLE (and Subtitle): SOLAR PUMPED LASER.	5. TYPE OF REPORT & PERIOD COVERED: FINAL TECHNICAL REPORT, 18 Feb [illegible] 74-11 Jul [illegible] 1975
	6. PERFORMING ORG. REPORT NUMBER
7. AUTHOR(s): Joseph D. Taynai	8. CONTRACT OR GRANT NUMBER(s): F33615-74-C-1062
9. PERFORMING ORGANIZATION NAME AND ADDRESS: GTE Sylvania, Inc. Electronic Systems Group - Western Division P.O. Box 188, Mountain View, California 94042	10. PROGRAM ELEMENT, PROJECT, TASK AREA & WORK UNIT NUMBERS: Project 2028 Task 01
11. CONTROLLING OFFICE NAME AND ADDRESS: Air Force Avionics Laboratory Air Force Systems Command Wright-Patterson AFB, Ohio 45433	12. REPORT DATE: Sept [illegible] 1976
	13. NUMBER OF PAGES: 103
14. MONITORING AGENCY NAME & ADDRESS (if different from Controlling Office)	15. SECURITY CLASS. (of this report): UNCLASSIFIED
	15a. DECLASSIFICATION/DOWNGRADING SCHEDULE

16. DISTRIBUTION STATEMENT (of this Report)

Distribution limited to U.S. Government agencies only; test and evaluation results reported, October 1975. Other requests for this document must be referred to the Air Force Avionics Laboratory (AFAL/DHO), Wright-Patterson AFB, Ohio 45433.

17. DISTRIBUTION STATEMENT (of the abstract entered in Block 20, if different from Report)

18. SUPPLEMENTARY NOTES

19. KEY WORDS (Continue on reverse side if necessary and identify by block number)

laser, Nd:YAG, Nd:Cr:YAG, solar pumping, mode locked, frequency doubled, space communication

micrometers

20. ABSTRACT (Continue on reverse side if necessary and identify by block number)

The objective of the work described in this report was the demonstration and delivery of a modelocked, frequency doubled, conductively cooled, solar pumped laser, designed to prototype space qualifiable level and structurally compatible with the EFM lamp pumped laser developed under AF contract No. F33615-74-C-1028. The laser was required to provide a minimum of 250 mW of 0.53μm radiation, mode locked at an average prf of 500 MHz with a pulse width of less than 300 ps. The laser actually produced 400 mW with 280 ps pulses with a Nd:Cr:YAG laser rod. Maximum power was 480 mW with 560 ps pulses.

DD FORM 1 JAN 73 1473 EDITION OF 1 NOV 65 IS OBSOLETE

UNCLASSIFIED

SECURITY CLASSIFICATION OF THIS PAGE (When Data Entered)

406 496

FOREWORD

This is the final report on work performed by the Electro-Optics Organization of GTE Sylvania, Inc, Mountain View, California for the Air Force Avionics Laboratory (TEL), Air Force Systems Command, Wright Patterson Air Force Base, Ohio, under Contract No. F33615-74-C-1062, Project 2028, Task 01. The work was performed during the period 18 February 1974 to 11 July 1975, for the Advanced Development Program 405B. Mr. Donald D. Matulka (AFAL/DHO-3) was the program monitor for the Avionics Laboratory.

This report was prepared by the Electro-Optics Organization of GTE Sylvania, Inc., Electronic Systems Group - Western Division, Mountain View, California and describes work performed in the Equipment Engineering Department headed by Mr. R. S. Reynolds. Dr. J. D. Taynai was the program manager. Laser development was performed by Dr. J. Falk, Mr. C. B. Hitz and Dr. Taynai. Dr. C. H. Chadwick was responsible for mechanical design and laser assembly; Mr. L. E. Wilson, for fabrication; Mr. H. Sweeney for all phases of the electronics. PSQM laser testing was performed by Mr. D. J. Radecki and Dr. E. Reed. Other contributions to the effort and assistance were provided by Messrs. E. J. Sleep, J. Becker, L. L. Schmidt and Mrs. M. B. Owen.

TABLE OF CONTENTS

LIST OF ILLUSTRATIONS

LIST OF ILLUSTRATION (Continued)

LIST OF TABLES

LIST OF TABLES (Continued)

Section I

INTRODUCTION

The Air Force, in its Advanced Development Program 405B, has been developing a laser system with which to evaluate experimentally a proposed optical communication system for use in space. The solar pumped laser is an important part of the system because of its low electrical input power requirement and its freedom from pump source lifetime limitations.

The first solar pumped laser program at GTE Sylvania[1] took place from January 1970 to August 1971. The result was the demonstration of a laser operating solar pumped, end pumped, conductively cooled, producing 1.05 watts of multimode power at 1.06μm. The second program[2] covered the time period December 1971 to July 1972. Several basic areas were investigated, and the modified laser produced 4.85 watts multimode and 0.8 watts TEM_{oo} mode, both at 1.06μm. The third[3] program began in January 1973, ending August 1973. A new laser was designed and fabricated incorporating features indicated by previous investigations, and providing an excellent test bed for further development. Nearly 6 watts of multimode output was obtained; 2.05 watts of TEM_{oo} mode output was also reported. At the second harmonic wavelength of 0.53μm, 0.43 watts cw output was obtained.

This, the fourth developmental program, began in Fabruary 1974, and experimental work continued until July 1975. The objective was the demonstration of a mode locked, frequency doubled, conductively cooled solar pumped laser, designed to prototype space qualifiable level and structurally compatible with the engineering feasibility model (EFM) lamp pumped laser, concurrently being developed under Air Force contract No. F33615-74-C-1028. The laser was to provide a minimum of 250 mW of mode locked output at 0.53μm, the second harmonic of the 1.06μm Nd:YAG laser wavelength. The mode locking frequency was to be 500 MHz; the pulse duration, less than 300 ps. The specifications are listed in Table 1.

The development portion of the program concentrated on laser resonator design and experimental optimization, laser rod doping selection, improvement in

Table 1

PSQM SOLAR PUMPED LASER SPECIFICATIONS

Wavelength - 0.53μm

Average Output Power - 250 mW minimum

- 400 mW goal

Average Output Power Stability - $\pm$2%, DC to 10^8 Hz

Mode - TEM_{oo}

Polarization - Plane, greater than 100:1

Mode Locked at 500 Mpps $\pm$50 Kpps, with rate of change less than 5 Kpps/sec

Pulse Duration - less than 300 ps, 10% rise to 90% fall

Clock Output - sinusoidal at laser prf, 0 dBm $\pm$1 dB into 50 ohm load, output VSWR less than 1.5. Phase variation relative to the optical pulse train less than $\pm 4.5^{o}$.

Rod Temperature - no less than $0^{o}C$

Laser Environment - 1g, $20^{o} \pm 5^{o}C$

Cooling Efficiency - greater than 95% through baseplates

Vibration Level - 15g design, 5g test

Conductively Cooled

No Phase Ambiguity

Utilize Cold Mirror Coatings

Interface with Solar Simulator and Solar Telescope

Interface with EFM Laser OMS

laser rod bonding and conductive cooling and determining parameters necessary for mechanical design of the PSQM laser. All phases of design, mechanical, electronic and optical, borrowed heavily from the EFM lamp pumped laser program. Most departures from that design resulted directly from the end pumping geometry used with solar pumping.

The PSQM laser incorporates an L shaped resonator cavity with one mirror, the laser rod, a light trap and an intracavity lens in one leg, a dichroic mirror and an acousto-optic mode locker frequency doubler (AOML/FD) in the other leg. The two legs are joined by a 45^{o} folding mirror which also serves to couple out the 0.53μm beam. The AOML/FD was developed by and procured from McDonnell Douglas Astronautics Company - East. The laser rod heat sink, light trap, and condensing cone account for most of the heat in the laser, and are conductively cooled by a single cold plate. All laser components are attached directly or indirectly to an invar laser structure. The laser resonator beam path is sealed to prevent dust, moisture or turbulence from affecting laser operation.

The laser produced 250 mW of ML/FD output with 280 ps pulse duration with a Nd:YAG laser rod; 400 mW with 280 ps pulse duration with a Nd:Cr:YAG rod. The highest power obtained was 480 mW with 560 ps pulse duration with the latter rod. The laser (Figure 1) performed best with a dielectric secondary mirror designed to reflect pump light from 0.43μm to 0.90μm to the laser rod, while transmitting or absorbing approximately 85% of the longer wavelength infrared radiation.

In addition to the basic PSQM laser effort, studies were made of coatings for use in space, effects of primary mirror deformation on pumping efficiency, and of the potential benefit of employing a YAG condensing cone rather than a hollow one. Also, lamp pumped laser pump cavities were fabricated and delivered for testing in conjunction with the EFM laser program.

Laser development is discussed in Section 2 of this report. The PSQM laser is described in Section 3 and results of laser testing presented in Section 4. Other tasks, mentioned in the previous paragraph, are discussed in Section 5. Summary and conclusions comprise Section 6.

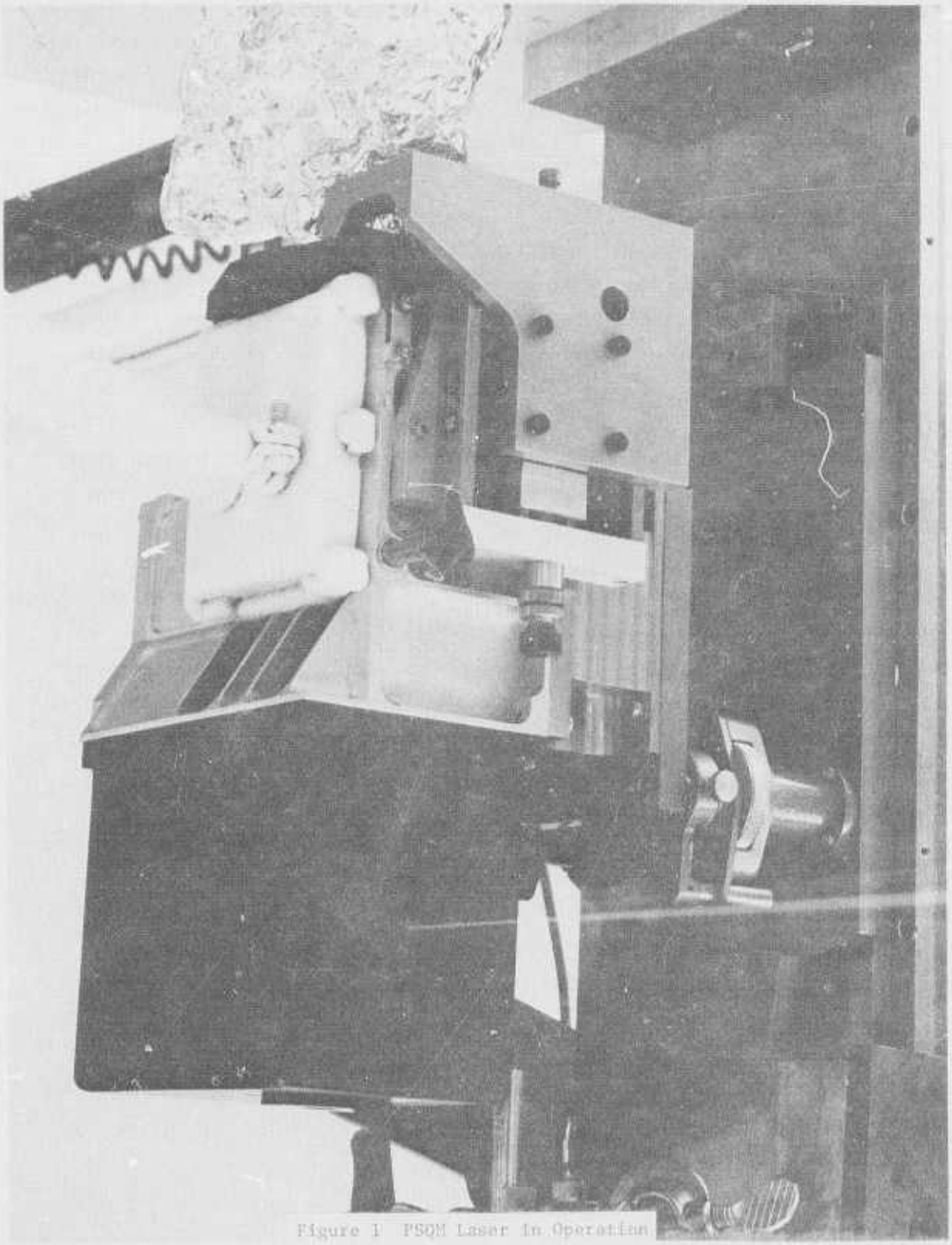

Figure 1 PSOM Laser In Operation

Section II

LASER DEVELOPMENT

2.1 Introduction

A portion of this program was devoted to development tasks, the outcome of which assisted laser mechanical design and choice of optical components for the PSQM laser. In addition, during the course of the planned development effort, several areas which needed investigation and understanding became evident.

The optical development performed on this program is discussed and described in Sections 2.4 and 2.5. However, much previous development was performed during the previous Sun Pumped Laser program[3], and the two lamp pumped laser programs, The Brassboard Laser Transmitter[4] and The Engineering Feasibility Model (EFM) Laser[5]. Work on the last mentioned program was performed just prior to corresponding portions of this one and much which led to particular designs for both programs is discussed in the EFM Laser Final Report[5]. Only the development actually performed on this program will be discussed at length in this report.

Section 2.2 discusses the difficulties encountered with the solar simulator, its limitations, and a comparison between it and the solar telescope. Power meter calibration is discussed in Section 2.3. Following that, laser rod tests and results are presented in Section 2.4. Finally, Section 2.5 covers the laser resonator tests.

The laser used for these tests was the one built on the previous program[3] and is shown in Figure 2. It is a good experimental test bed, having been designed to accommodate various laser resonator configurations and intracavity elements. Except for improvement in design, the developmental laser could be configured to be optically identical to the PSQM laser, so that optimization experiments could be meaningfully performed even while the detailed design and fabrication of the PSQM unit were in progress.

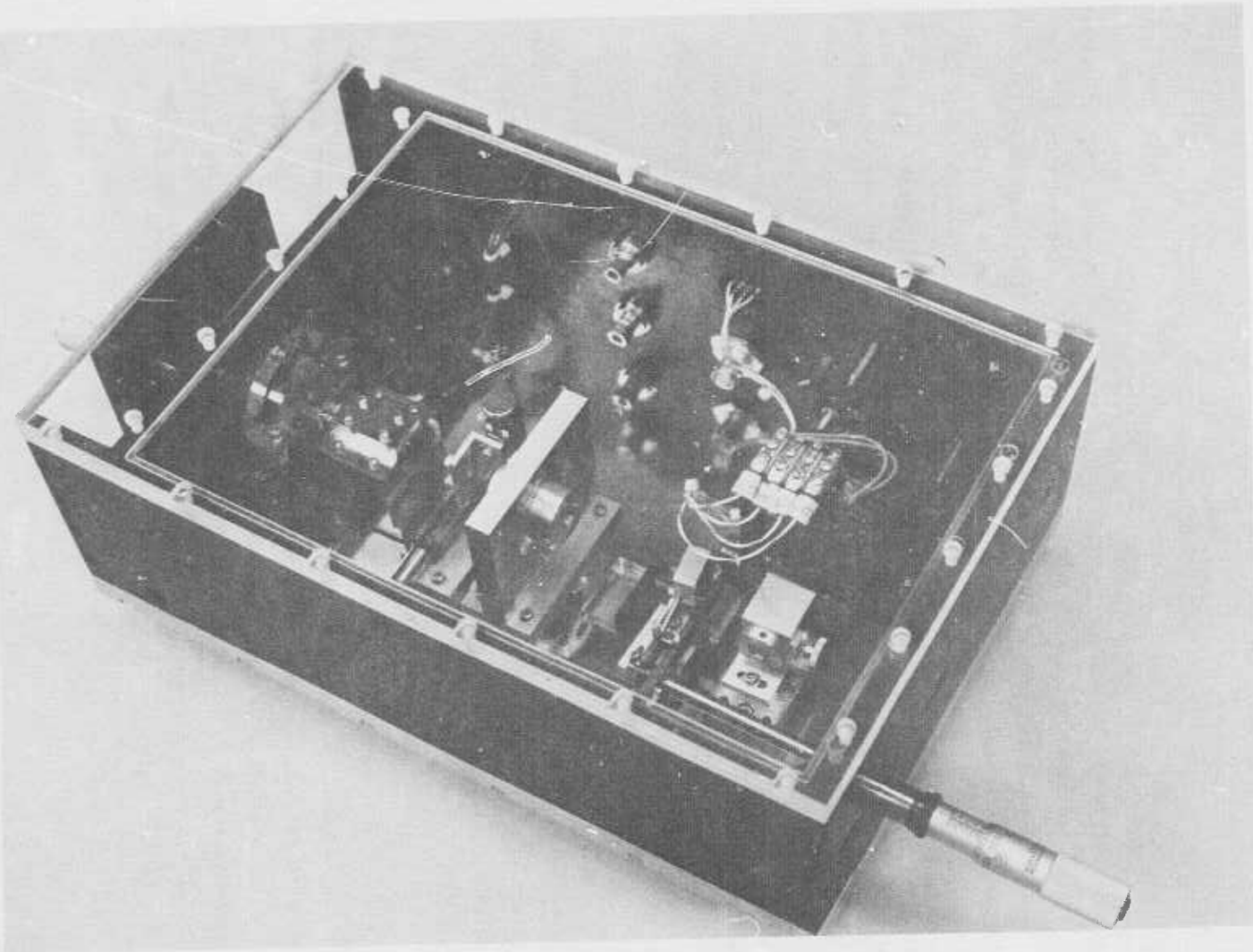

Figure 2 Developmental Model Solar Pumped Laser

2.2 Pump Sources - Solar Simulator and Solar Telescope

All developmental laser work done on this program was performed using the solar simulator, obtained on the last program.[3] The simulator consists of a lamphouse and a power supply, both shown in Figure 3. The lamphouse contains the 2 kW xenon short-arc lamp and an ellipsoidal reflector.

Lamp 1 is the original lamp, obtained and used on the last program and for the first part of this program. Lamps 2, 3 and 4 were obtained on this program. Lamp 1 exhibited erratic starting characteristics after 467 hours of operation. Inspection of the lamp showed the electrodes to be badly eroded, and the lamp envelope to be slightly discolored. Lamp 2 was installed, but the laser did not perform as well after the change. Careful inspection of lamp 2 showed the electrodes to be misaligned. Lamps 3 and 4 did not noticeably improve laser performance over that obtained with lamp 2, however. Some comparative testing was performed with lamp 3 despite this shortcoming.

Simulator output power measurements were made using a CRL Model 213 power meter, which is a water cooled, thermopile type device. Calibration data was available for the instrument used for measurements made on this program, but not for the original determination made on the last program. That data must be regarded as approximate only. There is significant variation between instruments, especially after long periods of usage or storage.

The measurements showed the output power with lamp 2 or 3 was less than 60% of that obtained previously. The cause of the power loss was found to be degradation of the ellipsoidal reflector. Careful inspection of the reflector showed a large portion of its surface to be discolored from its normal silver to shiny blue. The color indicates blue light is reflected noticeably better than yellow or red, and presumably infrared as well. Since all the primary pump bands of Nd:YAG and Nd:Cr:YAG are in the affected spectral region, this could easily account for the laser performance degradation. A new reflector was obtained and installed. The output power was improved to approximately the level previously produced by the simulator. The results are summarized in Table 2.

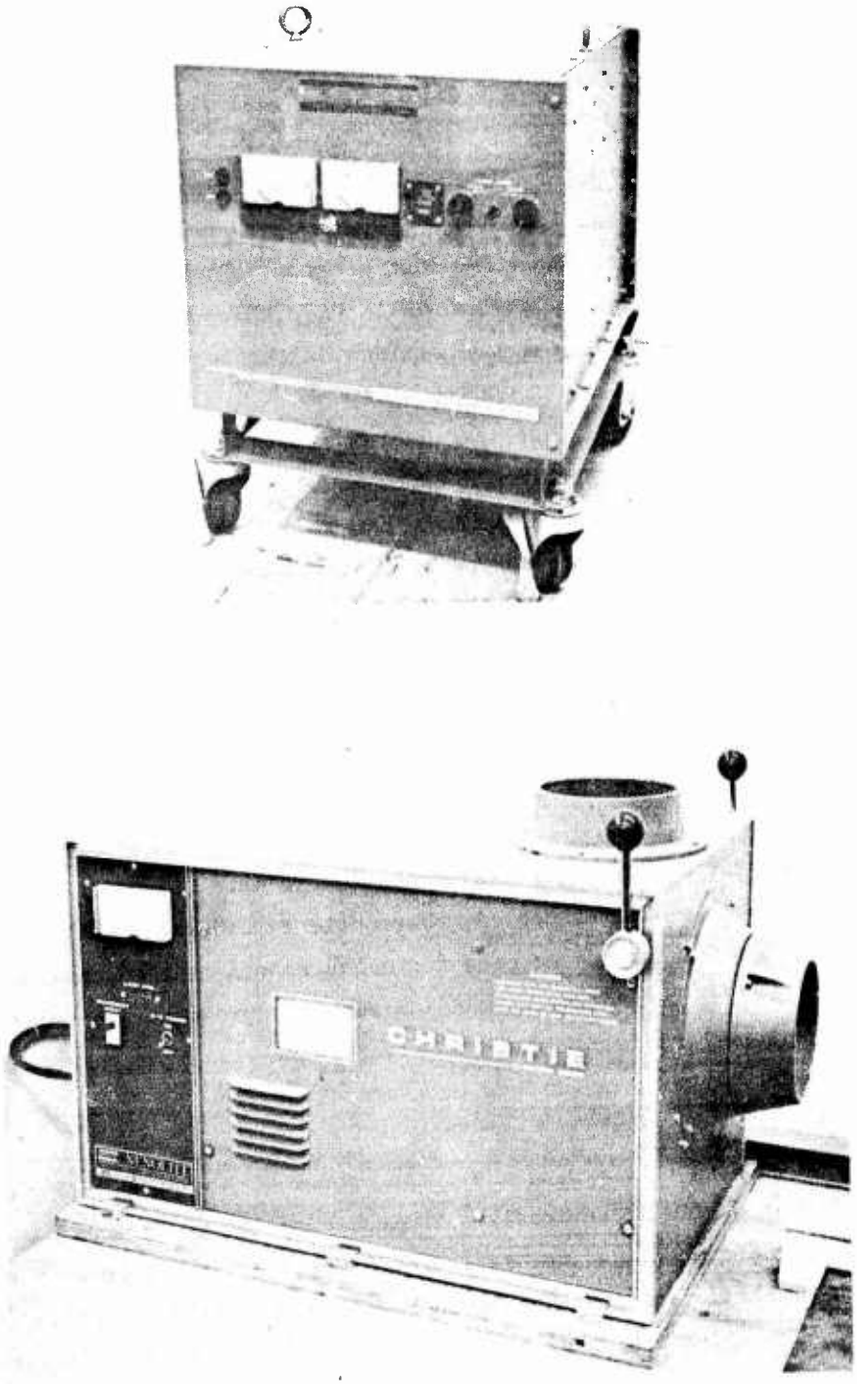

Figure 3 Photograph of the Solar Simulator Lamphouse and Power Supply

Table 2

SOLAR SIMULATOR OUTPUT POWER

Lamp Number	Date	Output Power	Comments
1	25 Jan. 1973	~400W	Uncalibrated meter
1	9 May 1974	370	-
2	16 Jan. 1975	230	-
3	16 Jan. 1975	232	-
3	21 Jan. 1975	385	New reflector

Input power approximately 2000W in all cases.

Table 3

COMPARATIVE LASER PERFORMANCE FOR SOLAR AND SIMULATOR PUMPING, ON THE PREVIOUS PROGRAM AND THIS ONE

	Simulator Pumped		Solar Pumped	
Program	Previous	Present	Previous	Present
MULTIMODE OUTPUT POWER	5.0W	3.2W	5.1W	4.8W
PUMP DRIVE LEVEL	(lamp input power) 2 KW	2 KW	(solar monitor reading) 7.2	6.6

Despite the restoration of simulator output power to the previous level, laser performance was still poorer than obtained previously. On the last program, the simulator driven at 2 kW lamp input power and the telescope at full aperture on a clear day with silver secondary mirror produced comparable multimode output power. Measurements made during this program, however, show that for the same laser rod, 931, while the solar telescope pumped laser output was nearly the same, the simulator pumped output was noticeably less. The results are summarized in Table 3. The solar monitor reading is the current produced by a silicon solar cell exposed to sunlight. This monitor is the same device used on the previous solar pumped laser program[3], and is described in Section 4.2 of this report.

Thus, total output power from the simulator is not a reliable measure of its pumping efficiency. Unless a simple reliable method can be found, the simulator should only be used for comparative measurements, and absolute, definitive results taken only using the solar telescope. Since the simulator is actually a movie projection light source and not a high quality, optically stable instrument, the limitation of its usefulness is reasonable.

By comparison, the solar telescope (see Figure 4) provides a more stable pumping beam than the simulator, since the lamp arc does wander and fluctuate in intensity. The telescope also provides a more sharply defined bright image with less peripheral light than the simulator. The spectrum of the pump light does not change as the telescope is apertured, while the spectrum of the simulator varies as the input power is changed. For a further discussion of the solar telescope and the solar simulator, see Reference 3.

The simulator, however, is more convenient to use, has a stable rather than a moving platform for the laser, and can be used regardless of weather and time of day. It is a useful tool, subject to its limitations, especially for comparative measurements and laser alignment.

Figure 4. Photograph of the Solar Telescope

The solar telescope, collecting the sun's rays at the earth's surface, provides a reasonable spectral approximation to the actual pump light to be found in space. The telescope also can accommodate various secondary mirrors, allowing filtering of the pump light prior to pumping. In this manner, unwanted long wavelength infrared radiation, which would only heat the laser rod, can be substantially reduced in intensity at the laser rod (discussed in Section 4.2).

2.3 Power Meter Calibration

The CRL Model 212 power meter has been used to measure both 1.06μm and 0.53μm laser output. During the course of the program, calibration of these power meters was investigated. It was found that the meters, as calibrated by the manufacturers at 1.06μm with a laser and a "standard" power meter, gave readings 20-25% higher than Eppley thermopiles, calibrated with an incoherent standard source. Apparently no accurate accepted calibration exists in the laser industry, and none traceable to the National Bureau of Standards (NBS).

NBS recently calibrated a CRL Model 201 power meter, a thermopile instrument, and sent it out for testing to six different experimenters. The consensus of their results was that the meter read 5% high[6].

To date, we have used CRL meters with their attendant calibrations. The results included in this report will be based on these calibrations. While there may be a multiplicative error in quoted results, the numbers will be accurate for relative comparison. Also, total communication system results depend not on power calibration, but on photoelectrons required per bit of information for a given maximum error rate. This is independent of the power standard.

2.4 Laser Rod Experiments

2.4.1 Rod Doping

To optimize laser performance, it was necessary to determine the Nd and Cr doping concentrations which would produce the highest laser output power. In order to accomplish this, the various laser rods available were compared early in the program. The rods were operated in the developmental model laser, configured for straight

cavity, multimode operation as shown in Figure 5. The laser was solar simulator pumped at 2 kW input to the lamp, the mirror separation was approximately 30 cm and the output mirror had a 60 cm radius of curvature and was 2.5% transmissive. All rods were anti-reflection (AR) coated for normal incidence at 1.064μm.

The results are summarized in Table 4 for those rods tested on this and the previous program. The degradation in output power attributed to the simulator in Section 2.2 is apparent, although the almost negligible decrease found with rod 931 does not fit the general pattern. Note that the decrease with the first two rods, doped with Nd only, is greater than that observed with two Nd:Cr rods (21-D and 107). A decrease in red and infrared reflectivity, as manifested by the blue color of the degraded simulator ellipsoidal reflector, would affect the Nd:YAG rods more than the Nd:Cr:YAG rods, since the Cr absorption occurs at shorter wavelengths.

While these rods represent a small sample space, especially considering rod-to-rod variation among supposedly identical rods, a decision was made based on the results. Four Nd:Cr:YAG rods of 1.0% Nd and 0.1% Cr concentration would be obtained. As a backup, four additional Nd:YAG rods with 1.0% Nd also were obtained.

The new rods were tested under the above conditions. The results are shown in Table 5. Two comparison runs were made because of the large number of rods and a limited number of heat sinks. The simulator reflector was replaced in the time interval between the two runs, which accounts for the large power disparity.

In summary, the new Nd:Cr:YAG rods are all inferior to rod 107, and all new Nd:YAG rods are all inferior to rod 4-27A. Rod 931 cannot be used in the PSQM laser since it is only 25 mm long. Thus, rods 107 and 4-27A were designated as candidate rods to be used in the PSQM laser.

2.4.2 Rod Focal Length

Because of the change in index of refraction of YAG with temperature, a rod of nonuniform temperature will exhibit prisming, lensing and higher order effects. Because the laser rod is approximately radially cooled (see Section 2.4.3), there is little linear temperature gradient, which would manifest itself as prisming. Such prisming, in which the laser rod acts as a prism or wedge, introduces no distortion in the beam.

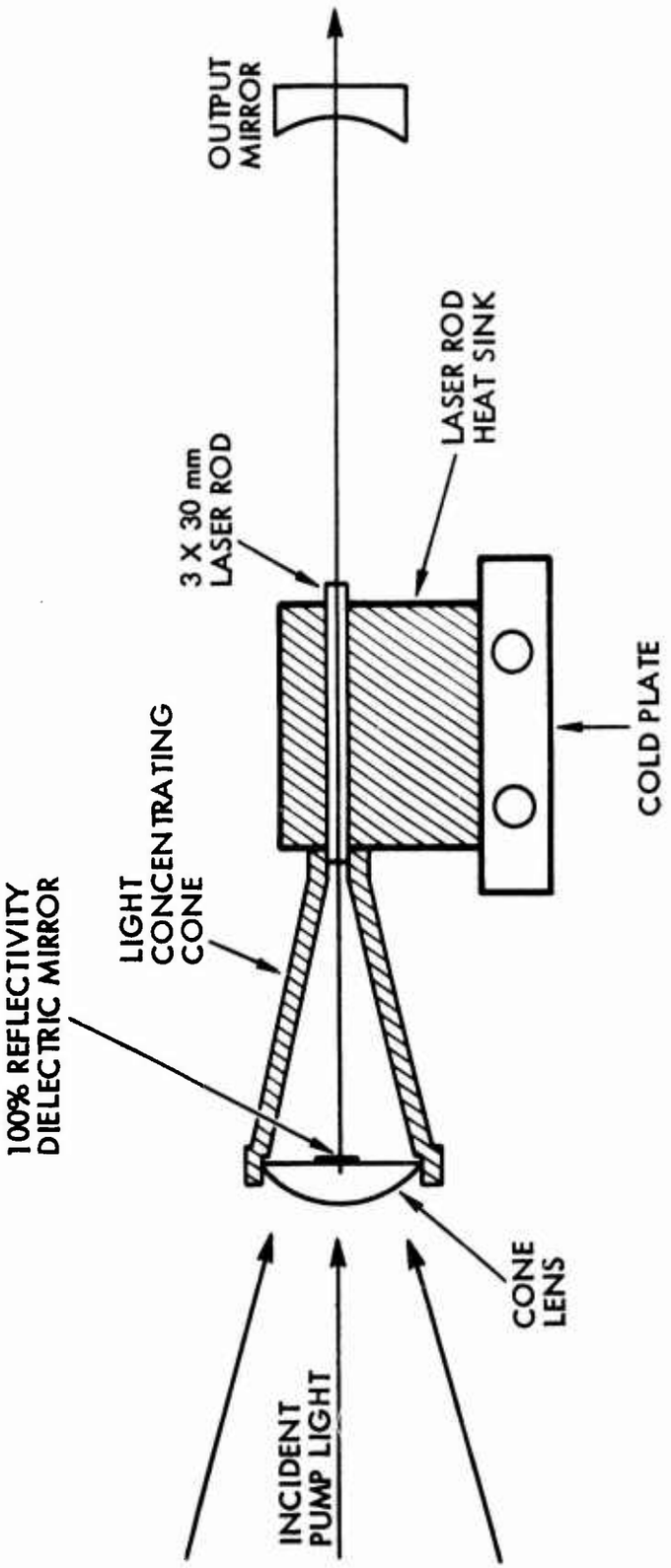

Figure 5 Laser Resonator Schematic for Straight Cavity Operation

Table 4

Multimode Comparison of Solar Simulator Pumped
Laser Rods for Doping Optimization

Rod Number	% Nd	% Cr	Multimode Output Power (Watts)	
			Previous Programs	Present Program
1565	1.0	-	4.0	2.75
4-27A	1.3	-	4.0	2.80
1697	0.3	0.03	1.4	-
1698	0.3	0.03	0.6	-
21-D	0.9	0.2	3.8	2.98
107	1.0	0.1	4.1	3.62
931	1.0	0.1	5.1	4.95
1-51A	1.3	0.1	-	3.10
1-52A	1.4	0.4	-	1.46

Table 5

Multimode Comparison of Solar Simulator Pumped
Laser Rods for Choice of Rods for Use in the PSQM Laser

Rod Number	Multimode Output Power (Watts) Run 1	Run 2
3260 *	.50	-
3261 *	.71	2.43
3262 *	.82	2.48
3263 *	.80	2.64
3274	.12	1.68
3275	.27	-
3276	no lasing	-
3277	.31	1.80
107 *	-	2.89
931 *	1.29	-
21-D *	.90	-
1-51A *	-	1.19
4-37A	-	2.28

* Nd:Cr double doped rods

Higher order spatial changes of refractive index, especially radial, introduce lensing. While the entire rod contributes to this lensing, it is distributed nonuniformly through the rod because of the axial gradient introduced by end pumping. It is necessary to determine the magnitude of this effect, since the resonator optical design is dependent upon it.

The lensing of the rod will manifest itself as does any cavity lens. The stability of the laser cavity can be calculated using the approach of Kogelnik and Li.[7] For each laser cavity element there is a 2 x 2 matrix which describes that element. The matrices can be used to determine if a configuration is stable. By translating the output mirror in Figure 5, the laser can be made to become unstable. By measuring the other parameters, the effective rod focal length can be determined.

The laser rod lensing is represented by a thin lens located at the midpoint of the rod. The matrices necessary are D_a for the distance from the flat mirror to the rod center, F for the unknown rod focal length, D_b for the distance from the rod center to the output mirror, and R for the output mirror. The quantities d_a and d_b are the optical distances mentioned above, f is the rod focal length, and r is the output mirror radius of curvature. The matrices are defined as follows:

$$D_a = \begin{pmatrix} 1 & d_a \\ 0 & 1 \end{pmatrix} \qquad D_b = \begin{pmatrix} 1 & d_b \\ 0 & 1 \end{pmatrix}$$

$$F = \begin{pmatrix} 1 & 0 \\ -\frac{1}{f} & 1 \end{pmatrix} \qquad R = \begin{pmatrix} 1 & 0 \\ -\frac{2}{r} & 1 \end{pmatrix}$$

The ABCD matrix is defined by the following matrix product.

$$\begin{pmatrix} A & B \\ C & D \end{pmatrix} = (D_a) \cdot (F) \cdot (D_b) \cdot (R) \cdot (D_b) \cdot (F) \cdot (D_a)$$

The stability criterion is $|(A + D)/2| \leq 1$.

The values of f for the crossover points between stability and instability are:

$$f = -r+d_b, \quad \frac{d_a d_b}{d_a - d_b}, \quad \frac{d_a(r - d_b)}{r - d_a - d_b}, \quad d_b$$

If the curvature of the output mirror is chosen so that r > f, then the procedure to find f is to move the output mirror away from the laser rod until the laser is operating intermittently and any further translation extinguishes the laser. To verify alignment, the mirror should be placed just beyond the extinguishing point, then the pump power should be decreased, decreasing the amount of focussing, increasing f. The laser should begin to oscillate. The solution for this case is the last one, d_b. In terms of actual parameters:

$$f = d + \frac{nd_r}{2}$$

where d is the rod to output mirror distance, d_r is the rod length and n is the rod index of refraction.

Simulator pumped at 2 kW lamp input power, a Nd:Cr:YAG rod had a 68 cm focal length; a Nd:YAG rod, a 78 cm focal length. Using the developmental laser with the solar telescope, at a solar reading of 7.0 with the wideband dielectric secondary mirror, Nd:YAG rod 4-27A had a 75 cm focal length; with the silver secondary, a 72 cm focal length. The simulator results only were available during the optical design effort described in Section 2.5.

2.4.3 Polarization and Rod Mounting

One of the specifications for the laser listed in Table 1 is that the output be plane polarized. The manner in which the laser is mode locked and frequency doubled, discussed in Section 2.5, requires that the 1.06μm beam in the resonator also be plane polarized. This is implemented by the properties of the folding mirror in the L-shaped resonator.

To optimize laser performance, it is necessary that the polarization introduce as small a loss as possible to the laser resonator. It was discovered on the previous program that a cylindrical laser rod which is uniformly end pumped but nonuniformly cooled on the cylindrical surface will provide higher output power for some forced polarization directions than for others. This is illustrated in Figure 6. This behavior was determined with the multimode cavity shown in Figure 5 with a rotatable Brewster plate polarizer inserted between the laser rod and the output mirror. The Brewster plate introduces sufficient loss to the orthogonal polarization to prevent it from oscillating, forcing the desired polarization.

Note that the maximum laser power does not occur at 0^{o} or vertical polarization in Figure 6, but about 12^{o} off vertical. Data for rod 107 and for rod 931 are shown in a polar plot in Figure 7. The patterns for both rods are sharply lobed, but the solid curve (rod 931) has its near-vertical maximum much closer to 0^{o} than the dashed curve (rod 107). For forced vertical polarization, one of the baseline design features, rod 931 would produce 95% of its maximum power, whereas rod 107 would produce only 50%. Ideally, the maximum output power should be produced for vertical polarization.

Figure 7 also shows an end view of the laser rod and its heat sink. The rod is soldered into the heat sink, and the heat is removed by conduction to a cold plate at the bottom. To make the soldering less difficult, the heat sink is split horizontally coinciding with the center of the laser rod. While the heat sink is made of copper, whose thermal conductivity ($4W/cm/^{o}K$) is much higher than that of the laser rod (.13), heat is not removed from the rod uniformly radially. If the heat were removed uniformly radially the uniformly end pumped rod should produce the same power for any polarization, since Nd:YAG, (and presumably Nd:Cr:YAG is isotropic.

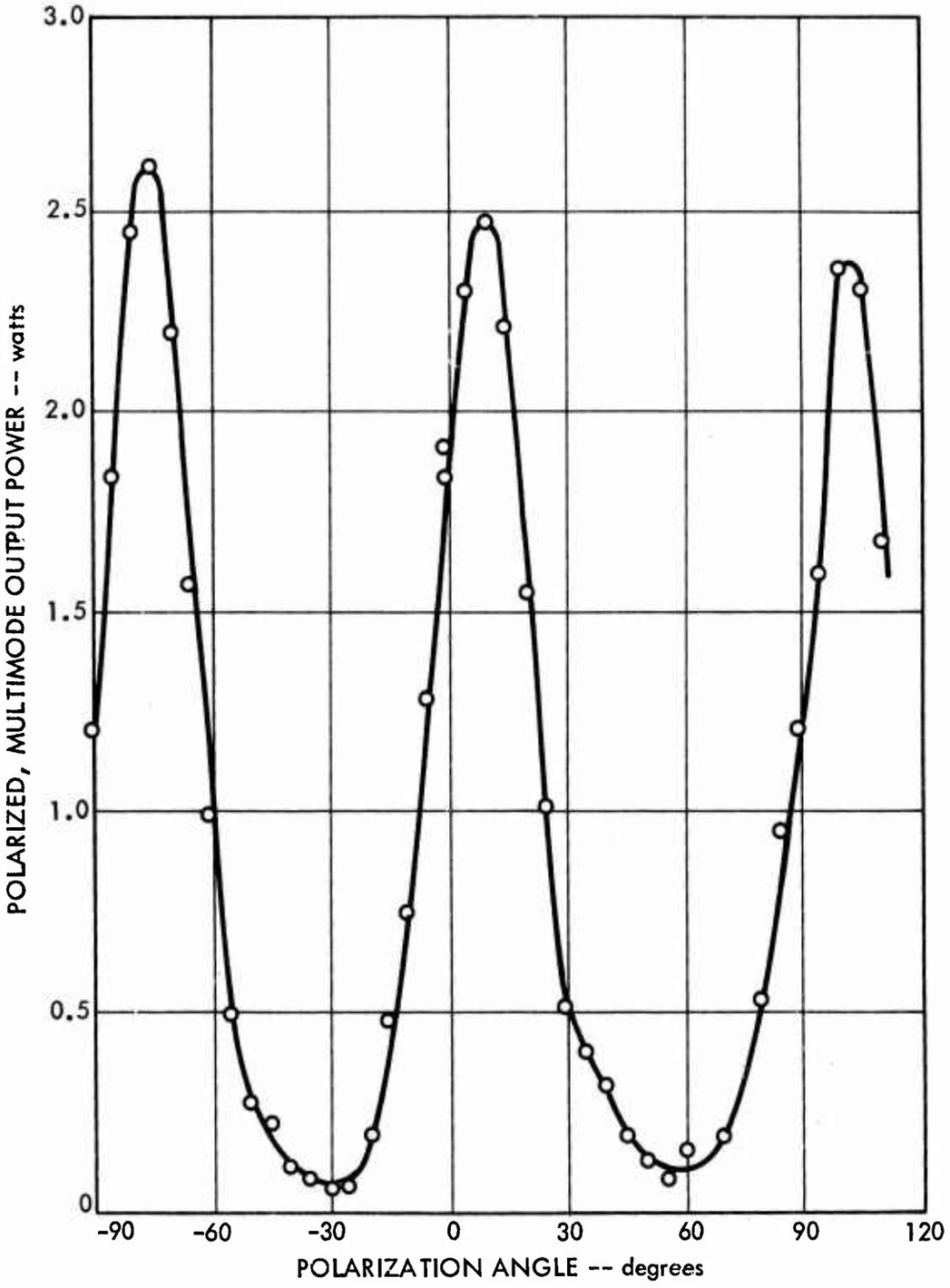

Figure 6 Polarized Multimode Output Power of Rod 107 as a Function of Polarization Direction

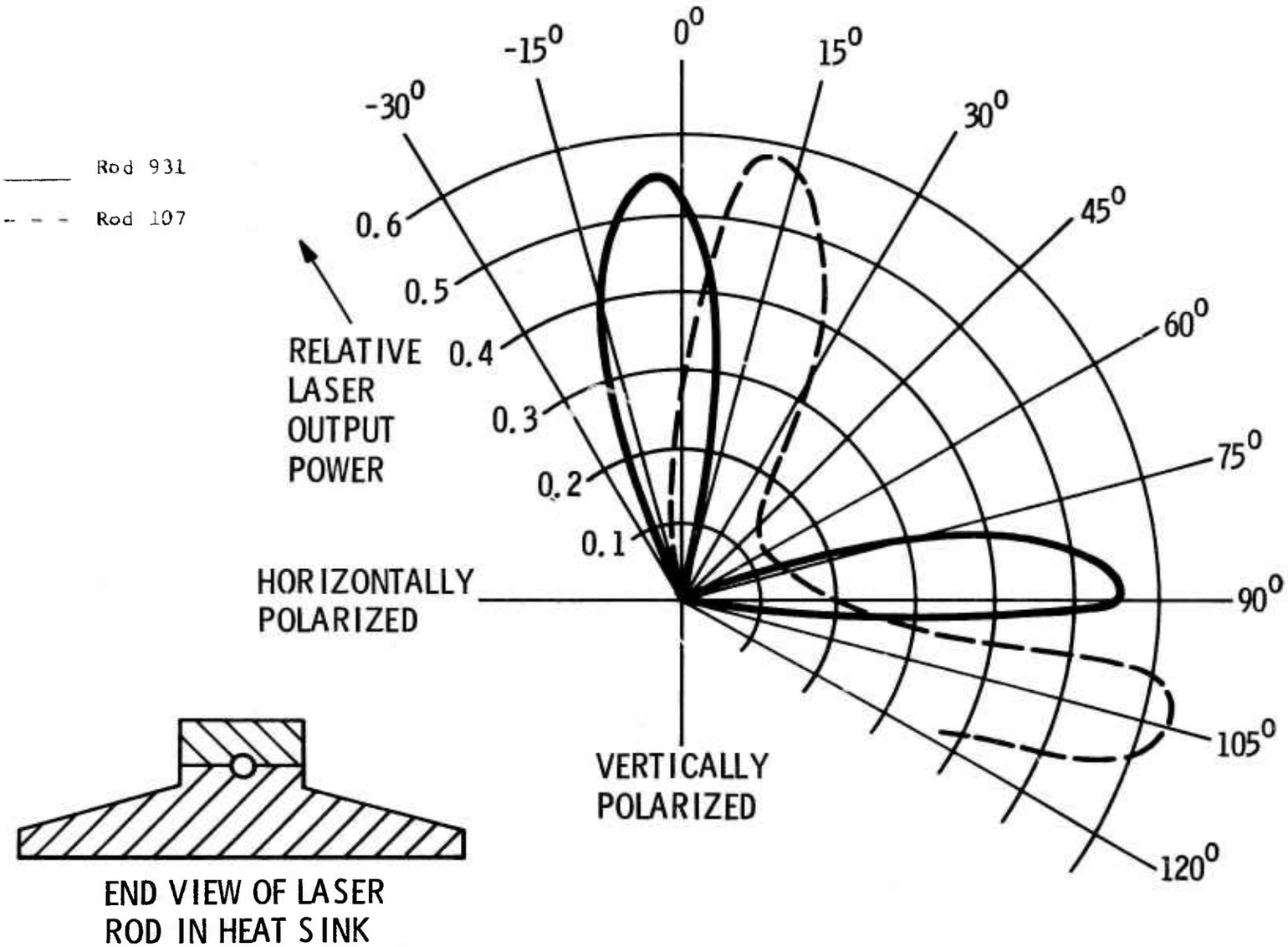

Figure 7 Polar Plot of Laser Output Power for Two Conductively Cooled Laser Rods as a Function of Forced Polarization

At the interface between the heat sink top and bottom, a temperature drop will develop for any measurable heat flow. This is caused by imperfect matching of the two machined surfaces and the presence of oxides and foreign substances. Thus, more heat is removed from the bottom half of the rod than from the top half. The heat stream lines and the isotherms would be symmetric about a vertical line through the center of the rod. From symmetry arguments alone, the polar output power plot should be symmetrical about the 0^{o} line.

It was decided to test whether a Nd:Cr:YAG rod was actually isotropic, as mentioned above. Rod 931 is such a rod, and its maximum (Figure 7) was very nearly vertical. 931 was heated in its heat sink to just above the solder melting point. The rod was then rotated carefully 45^{o} in the heat sink. The polar power plot of the rotated rod was unchanged. This was felt to be sufficient evidence that the laser materials used are isotropic, and the cause of the off vertical power maximum was not inherent to the rod.

While a number of laser rods exhibited the off vertical polarization preference, rod 107 was investigated to a greater extent than the others. Evaluation during the previous program had shown this rod to have produced the highest multimode output power (except for rod 931) and the highest polarized and unpolarized TEM_{oo} powers of any rod. Thus, 107 was potentially the best rod in our possession, and deserved special investigation.

Careful examination under a microscope showed rod 107 to be mounted asymmetrically in its heat sink, and the heat sink top and bottom to be misaligned, as shown by Figure 8. It was thought that these two features would destroy the vertical symmetry discussed above, and possibly cause the off vertical polarization preference.

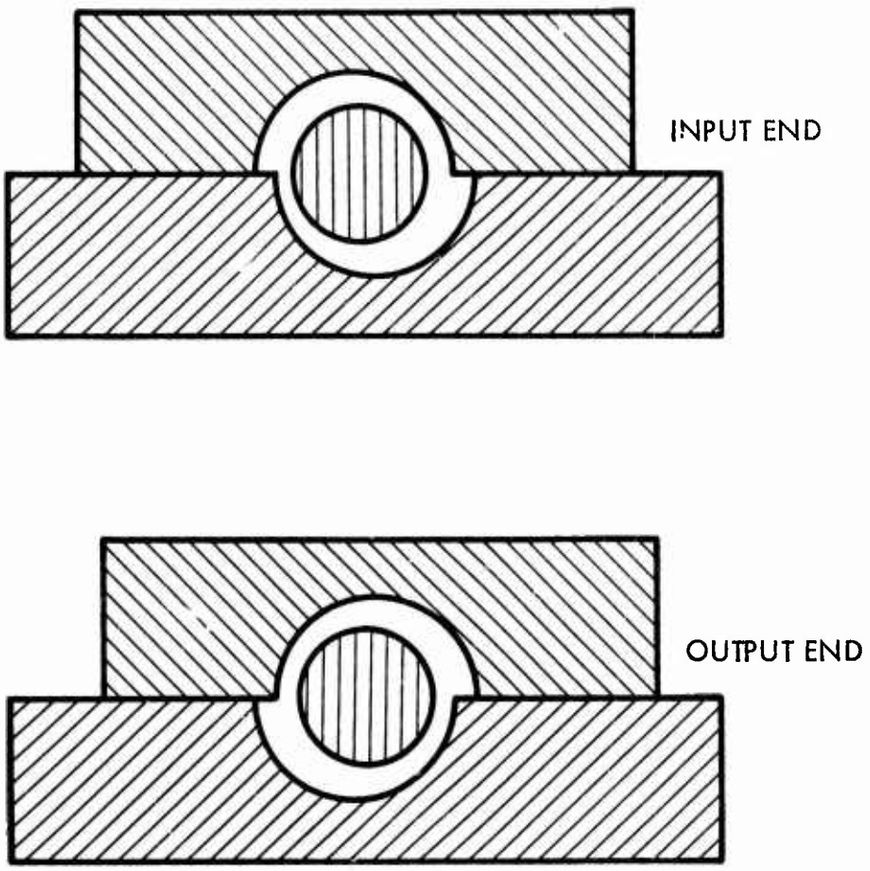

Figure 8 Drawing of Skew Mounting of Laser Rod 107

This led to a change in laser rod mounting hardware and procedure. Fixtures were made to center the rod in the cylindrical hole in the heat sink. The top of the heat sink was aligned with respect to the bottom with guide pins. The rod was placed in the channel of the bottom of the heat sink, the channel having been filled with indium and formed to the rod size and shape by impressing with a proper sized drill blank. The heat sink top, similarly pre-processed, was set atop the guide pins, which were sufficiently large to prevent the top from sliding in place. The assembly was then heated on a hot plate until the indium in the bottom channel melted and pulled the rod in place. The rod was translated back and forth along the channel to enhance the wetting, then the top was pushed down over the guide pins. As soon as the indium in the top channel melted, the two heat sink parts were fastened together with four bolts.

Several rods mounted with this procedure showed inconclusive results. Dismounting them revealed insufficient wetting of the upper half of the rod by the indium in the channel. The procedure was modified to remedy this. The guide pin holes were enlarged sufficiently to allow a slip fit between the pins and heat sink. The pins were not installed at first. The rod could now be translated slightly with respect to both parts of the heat sink to improve wettability. The pins were installed just prior to cooling the assembly to freeze the indium solder.

The results of this testing are summarized in Table 6. Rod 107 produced poor results for the final mounting procedure because the metallization on the rod had degraded. This rod and its peculiarities are discussed below. Rod 931 is only 25 mm long, and could not be used in the PSQM laser, which was designed around a 30 mm long rod. It was used for comparison purposes during the testing, and for the rod rotation test. The eight rods obtained during this program were mounted after adoption of the use of rod centering and guide pins.

Table 6

Summary of Laser Rod Polarization Preference with Respect to Vertical for Three Different Mounting Techniques

Laser Rod	Position of Maximum Polarized Power			Comments
	Mount 1	Mount 2	Mount 3	
107	12^{o}	8^{o}	30^{o}	Metallization degraded in #3
931	$5^{o}/3^{o}$	-	-	25mm rod. Before and after 45^{o} rotation in #1
21-D	5^{o}	12^{o}	0^{o}	
1-51A	-	12^{o}	10^{o}	
4-27A	$35^{o}/3^{o}$	10^{o}	0^{o}	Rod centering, annealling in #1
3260	-	-	-	Inferior Rod
3261	-	17^{o}	0^{o}	
3262	-	12^{o}	0^{o}	
3263	-	10^{o}	0^{o}	
3274	-	7^{o}	0^{o}	
3275	-	-	0^{o}	
3276	-	-	-	Never lased
3277	-	17^{o}	0^{o}	

Mount 1 - No rod centering, no guide pins.

Mount 2 - Rod centering, guide pins at start.

Mount 3 - Rod centering, guide pins installed last.

Rod 107 resisted all attempts to obtain maximum power for vertical polarization. It was remounted several times using the final technique, with the resulting maximum power direction being approximately 10^{o} off vertical, in the same direction each time. Since all the rods had 0.5^{o} canted ends, repeated alignment was possible. Finally, the rod was mounted rotationally offset $\sim 10^{o}$ in the direction which would rotate the pattern to vertical if the pattern were associated with the laser rod. The rod exhibited a maximum polarization orientation of approximately $2\text{-}1/2^{o}$ off vertical, with less than a 6% reduction in power for forced vertical polarization. While the behavior of this rod is not well understood, it was decided not to pursue the investigation, especially since an acceptable mounting had been accomplished.

Using the procedure described above Nd:YAG rod 4-27A and Nd:Cr:YAG rod 107 were mounted for testing in the PSQM laser.

A copper heat sink was electroformed to laser rod 1565, but coating damage and a shortage of time precluded evaluation. Rod 1-52A was mounted using a thermally conductive epoxy, but evaluation proved inconclusive.

2.5 Laser Resonator

2.5.1 Description of the Resonator

The laser incorporates an L shaped resonator cavity with an HR mirror, the laser rod, a light trap and an intracavity lens in one leg, a dichroic mirror and an acousto-optic mode locker, frequency doubler (AOML/FD) in the other leg. The two legs are joined by a 45^{o} folding mirror which also serves to couple out the 0.53μm beam. The resonator shown schematically in Figure 9 is quite similar to that of the EFM lamp pumped laser[5]. The 1.06μm beam is virtually collimated in the region from the HR 1.06μm mirror M_1 through the laser rod to the intracavity lens. The lens focusses the beam so that it is converging toward the right and downward in Figure 2, following its reflection from folding mirror M_2. The beam creates a focus at or near the barium sodium niobate (chemical representation $Ba_2Na(N_bO_3)_5$, often abbreviated BSN) crystal, which is used to mode lock and frequency double the laser. The dichroic mirror, M_3, serves to terminate the cavity.

The 1.06μm beam resonates in both legs of the L. The BSN crystal, functioning as a loss modulator, mode locks the 1.06μm beam at a pulse repetition frequency equal to c/2L, where c is the speed of light and L is the cavity optical length. The 1.06μm pulse generates 0.53μm radiation in the BSN crystal, functioning as a frequency doubler, on both passes (in both directions) through the crystal. Mirror M_3 allows the two oppositely directed 0.53μm beams to be coherently combined, and to exit the cavity at mirror M_2.

The laser operates with the 1.06μm beam linearly polarized vertically, normal to the plane of the L. Linear polarization is required because of the frequency doubling properties of the BSN crystal. The crystal is oriented in the resonator to convert the polarized 1.06μm radiation to orthogonally polarized (parallel to the plane of the L) 0.53μm radiation. The folding mirror M_2 in Figure 9 is dielectrically coated to transmit (T > 90%) of the 0.53μm radiation polarized parallel to the plane of the L, yet reflect virtually all of the orthogonally polarized 1.06μm radiation.

Several constraints of end pumping cause the solar pumped laser resonator to differ from that of the EFM lamp pumped laser. Mirror M_1 is deposited on the plane surface of the plano-convex cone lens, and is constrained to be flat for this laser. Any departure would introduce greater complexity and higher cost for the pumping end of the laser. A 3mm diameter rod is used to maximize gain, subject to limitations discussed in Section 2.4. Since the EFM laser rod is 4mm in diameter, the solar pumped laser will have a smaller beam diameter in the collimated section of the resonator. While a 30mm long rod is used in this laser, compared to 63.5mm for the EFM laser rod, the axial nature of the pump light necessitates its removal from the resonator with a light trap between the rod and the intracavity lens. This element limits the minimum rod/lens spacing.

2.5.2 Optical Design

The theory of optical design of the resonator and optimization of the laser performance was not originated on this program. It was developed and applied first for the lamp pumped laser and further discussion of various aspects of the design can be found in other reports[4,5]. An overview will be presented here.

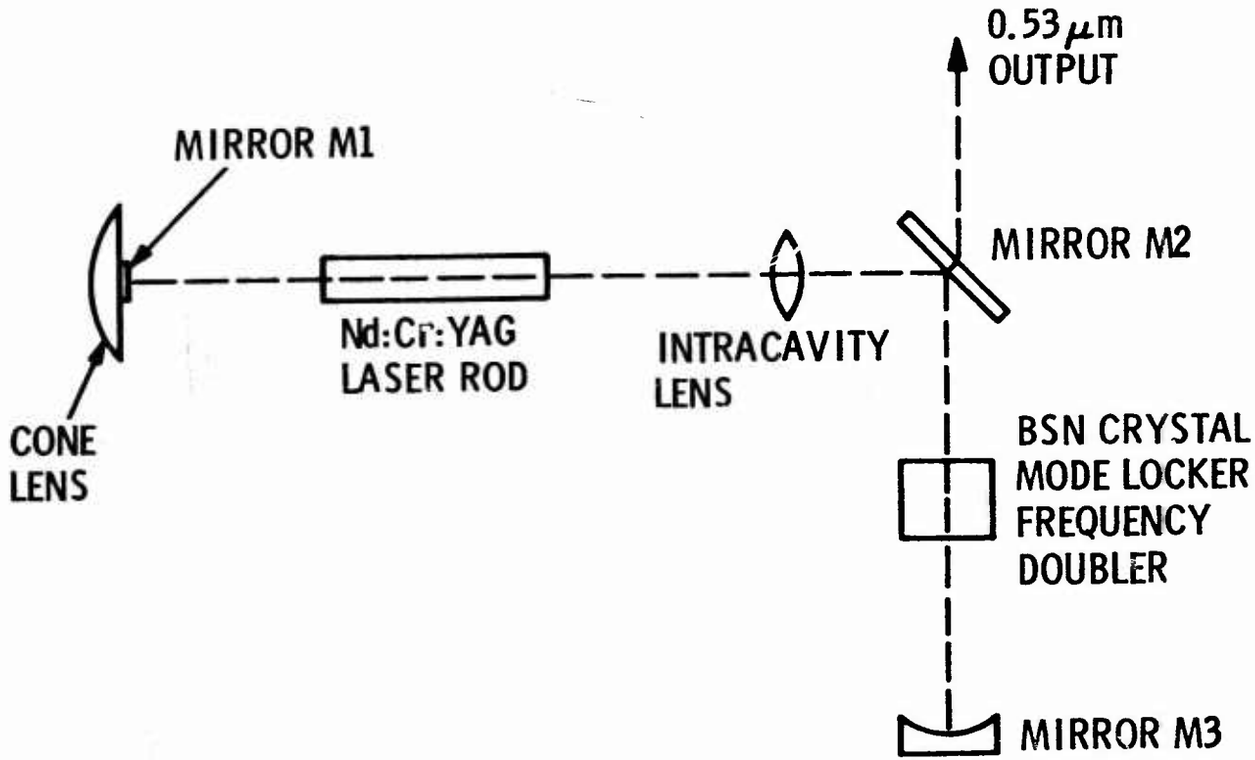

Figure 9 Laser Resonator Schematic

Using the ABCD matrices of Kogelnik and Li[7] similarly to the manner discussed in Section 2.4.2, the beam within the resonator can be described. The fixed input characteristics are: total resonator optical length; flat mirror M_1; fixed distance between M_1 and the laser rod; minimum distance between the rod and the intracavity lens; minimum distance between the BSN crystal and the dichroic mirror M_2; effective laser rod focal length (Section 2.4.2); effective BSN crystal focal length. Two parameters of extreme importance are beam diameter in the laser rod, and in the BSN crystal. The first is critical, since if the beam is too large, aperturing by the laser rod edge and heat sink will provide excessive loss; conversely, if the beam is too small, modes of order higher than TEM_{oo} will also oscillate.

The beam diameter at the BSN crystal is critical for both mode locking and frequency doubling. A large beam will couple inefficiently for frequency doubling because the power per unit area is low, and also may be too large for the acoustic column in the crystal for effective mode locking. Too small a beam would cause the pulse duration to be too long because of overcoupling. Also, too small a spot would decrease mode locking efficiency since the small spot-corresponds to a large spread in photon k vector, some of the distribution being outside the acceptance cone for Bragg diffraction mode locking.

From experience, a beam diameter of approximately 1/3 of the laser rod diameter corresponds to the highest TRM_{oo} mode circulating power in the cavity. This appears to be true for both side pumped and end pumped laser rods. Thus, an a priori "constraint" was imposed of approximately 1mm TEM_{oo} mode diameter in the laser rod.

For the beam diameter in the BSN crystal, the beam diameter was constrained to be less than the 0.5mm acoustic column used for mode locking, and greater than the approximately 0.1mm limit corresponding to too large a k vector spread.

The variables in the theoretical design are intracavity lens focal length and position, and dichroic mirror radius of curvature. For a given lens focal length and mirror curvature, the mathematical model[5] predicts beam sizes in the rod and BSN crystal for each lens position. By varying the lens position, a curve for the beam size at the rod and BSN crystal can be generated by changing lens focal length or mirror curvature.

A typical family of curves is shown in Figure 10. The upper curves are for laser rod beam diameter for three different mirror curvatures. When the curves become steep, small changes in lens position could extinguish the laser by requiring too large a mode diameter. When the curves are flat, lens position affects rod mode diameter very little. Each lens/mirror combination has a minimum rod mode diameter.

Sets of curves like Figure 10 were used to generate a large number of possible laser resonators. A number of these are summarized in Table 7. For these cavities, the rod mode diameter was 1mm and the M_1 to laser rod distance fixed at 4.25 cm. For the last five cavities, the beam waist in the frequency doubling leg occurs at the BSN crystal center; for the first five, the waist is displaced to allow a larger BSN beam diameter for a smaller waist diameter.

2.5.3 Acousto-Optic Mode Locker/Frequency Doubler

Developed by and procured from McDonnell Douglas Astronautics Company - East (MDAC), the acousto-optic mode locker/frequency doubler (AOML/FD) is a key item in the solar pumped laser. The unit contains a barium sodium niobate crystal which is used to simultaneously mode lock and frequency double the 1.06μm laser beam. The crystal is coated to have virtually zero loss at 1.06μm and as low a loss at 0.53μm consistent with the first condition. A specially applied transducer generates an acoustic column in the crystal for mode locking. The crystal is contained within an oven for temperature control for frequency doubling.

Four AOML/FD's were used on this program, three with the developmental laser and one with the PSQM laser. The first, provided as GFE, was an early model and was not able to be used to produce satisfactory ML/FD operation. The second, unit D-11, was purchased on this program for developmental purposes. It was found that the acoustic column width varied from over 400μm (expected value) to less than 250μm. Also, the diffraction efficiency was a strong function of position in the crystal, and crystal temperature.

The devices produced up to that time were designed to be acoustically resonant, to improve the diffraction efficiency. It was found that maintaining the diffraction efficiency and frequency doubling efficiency at high levels simultaneously was virtually impossible. It was decided that modifying the device to

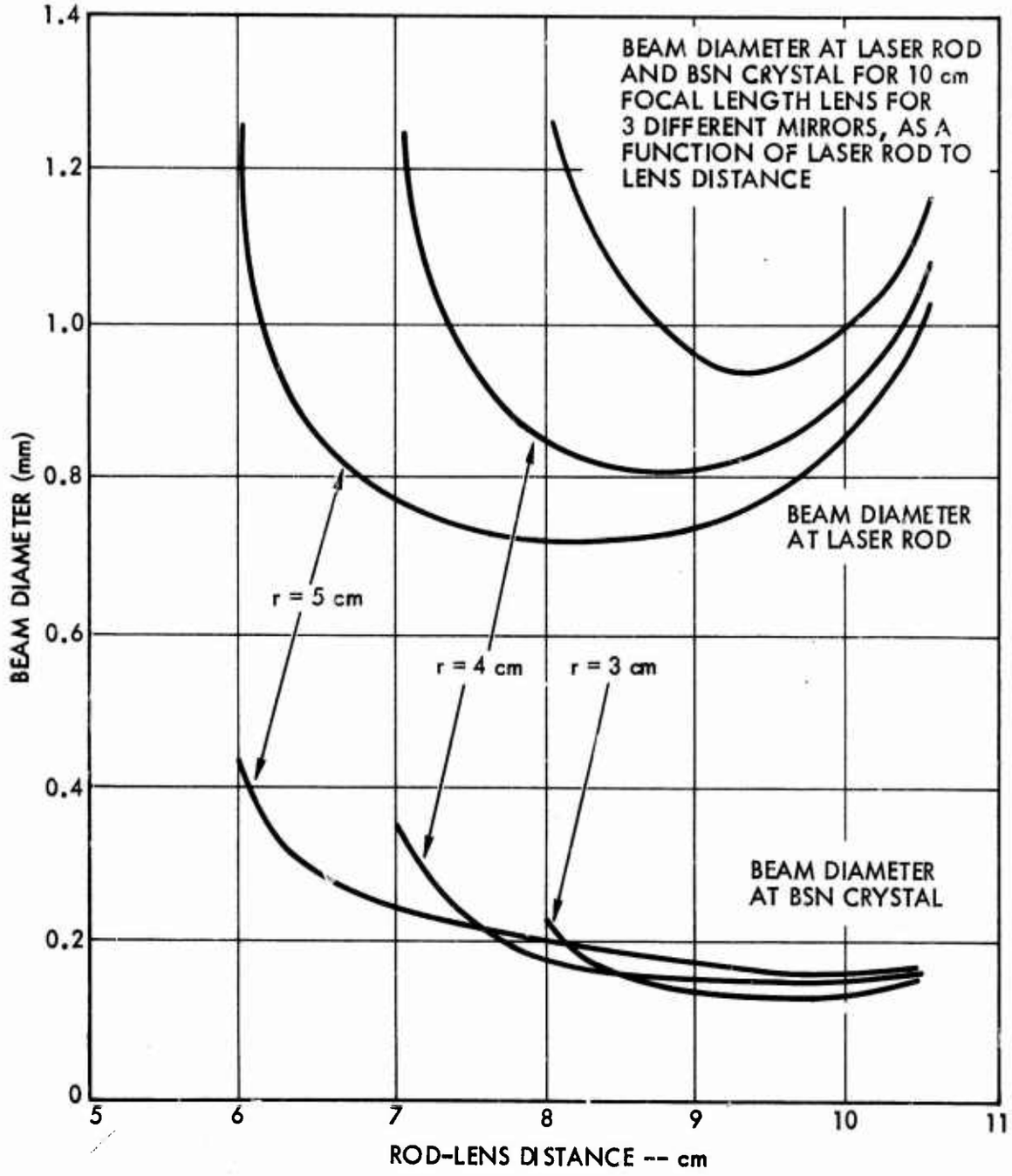

Figure 10 Typical Resonator Cavity Design Curves

Table 7

Theoretical Laser Resonator Parameters

Lens Focal Length (cm)	Dichroic Mirror Radius of Curvature (cm)	Rod to Lens Distance (cm)	Beam Diameter in BSN Crystal (μm)
14	7	1.7	434
12	6	3.9	396
14	6	2.9	342
16	6	2.0	308
14	5	4.2	256
16	7	5.4	198
14	5	6.65	178
12	4	8.5	160
10	3	9.4	142
7.5	2	11.2	106

Laser Rod Beam Diameter is 1.0mm

be acoustically non-resonant would improve its performance, so D-11 was returned to MDAC for this purpose. Subsequent testing indeed showed improved performance. The unit was used until the crystal was accidentally damaged, apparently by sudden application of RF drive power for mode locking. Development was completed using unit D-12, borrowed as GFE and returned when the PSQM laser was operational.

Despite the change to acoustic non-resonant operation, the AOML/FD units need further development. Combination of mode locking (acoustically controlled) and frequency doubling (thermally controlled) within the same crystal does not allow independent adjustment and maximizing of both functions. Crystal temperature changes were caused by variations in 1.06μm generation and thence 1.06μm and 0.53μm absorption in the crystal, by variation of the frequency doubling oven temperature, by variation of the absorbed acoustic energy needed for mode locking, and also by changes in laser ambient conditions. These temperature variations caused further changes in mode locking and frequency doubling, especially when the laser was operated outdoors with the solar telescope. Further discussion of the device and its characteristics can be found in the EFM laser final report[5].

Unit D-20 was purchased from MDAC for use in the PSQM laser. It had a measured diffraction efficiency of approximately 4.6% at 2 watts drive, and less than 0.3% insertion loss. The sound column width was found to be greater than 425μm at 0.9 watts RF drive and greater than 600μm for 1.7 watts drive. The unit performed satisfactorily in the PSQM laser, producing 400 mW of mode locked, frequency doubled output with 280 psec pulses. The unit is shown in its mount in Figure 15, in Section 3.5.

2.5.4 Development Results

The candidate resonator configurations were evaluated with the simulator pumped developmental model laser (Figure 2). Difficulties were experienced because of solar simulator degradation and general unreliability. Despite this, the testing was finally completed, with the laser producing approximately 200 mW of mode locked, frequency doubled output with less than 300 psec pulses. The resonator used for this contained a 6 cm radius of curvature dichroic mirror, a 13 cm focal length lens, and Nd:YAG laser rod 4-27A. Nd:Cr:YAG rod 107 was not useable at that time because of mounting and polarization difficulties (Section 2.4.3).

It was realized that changing to solar pumping and the use of a Nd:Cr:YAG rod would necessitate further testing.

Section III

DESCRIPTION OF THE PSQM LASER

3.1 Introduction

The PSQM solar pumped laser was designed using applicable PSQM lamp pumped laser design, discussed in Section 3.2. Several subassemblies are virtually identical to those in this lamp pumped laser, including the dichroic mirror mount, the AOML/FD mount, the lens mount, the folding mirror mount, and the clock detector mechanical assembly.

The solar pumped laser schematic, including the solar telescope, is shown in Figure 11. Those portions peculiar to the solar pumped laser are directly involved with end pumping of the laser rod. These are discussed in Section 3.3.

The pumping and cooling subassembly is discussed in Section 3.4, the various mounts in Section 3.5, and the laser structure in Section 3.6. The assembled laser is discussed in Section 3.7, and the electronics in Section 3.8.

3.2 Applicable Lamp Pumped Laser Design

Paralleling the solar pumped laser development over the last several years, the K-Rb lamp pumped laser has progressed from laboratory demonstration model (Space Laser Design, contract No. F33615-72-C-1629)[8] through the brassboard stage (Brassboard Laser Transmitter, contract No. F33615-73-C-1140)[4] to the just completed PSQM Laser (Engineering Feasibility Model contract No. Y3E-247[5]). Most of the design approaches, much of the specific technology and many of the specific designs of the lamp pumped laser effort have been directly applicable to the PSQM solar pumped laser. The present program was predicated upon the usefulness of lamp pumped laser design and economy of the commonality of the two lasers. Because of this, a greater portion of the program could be dedicated to those features peculiar to solar pumping.

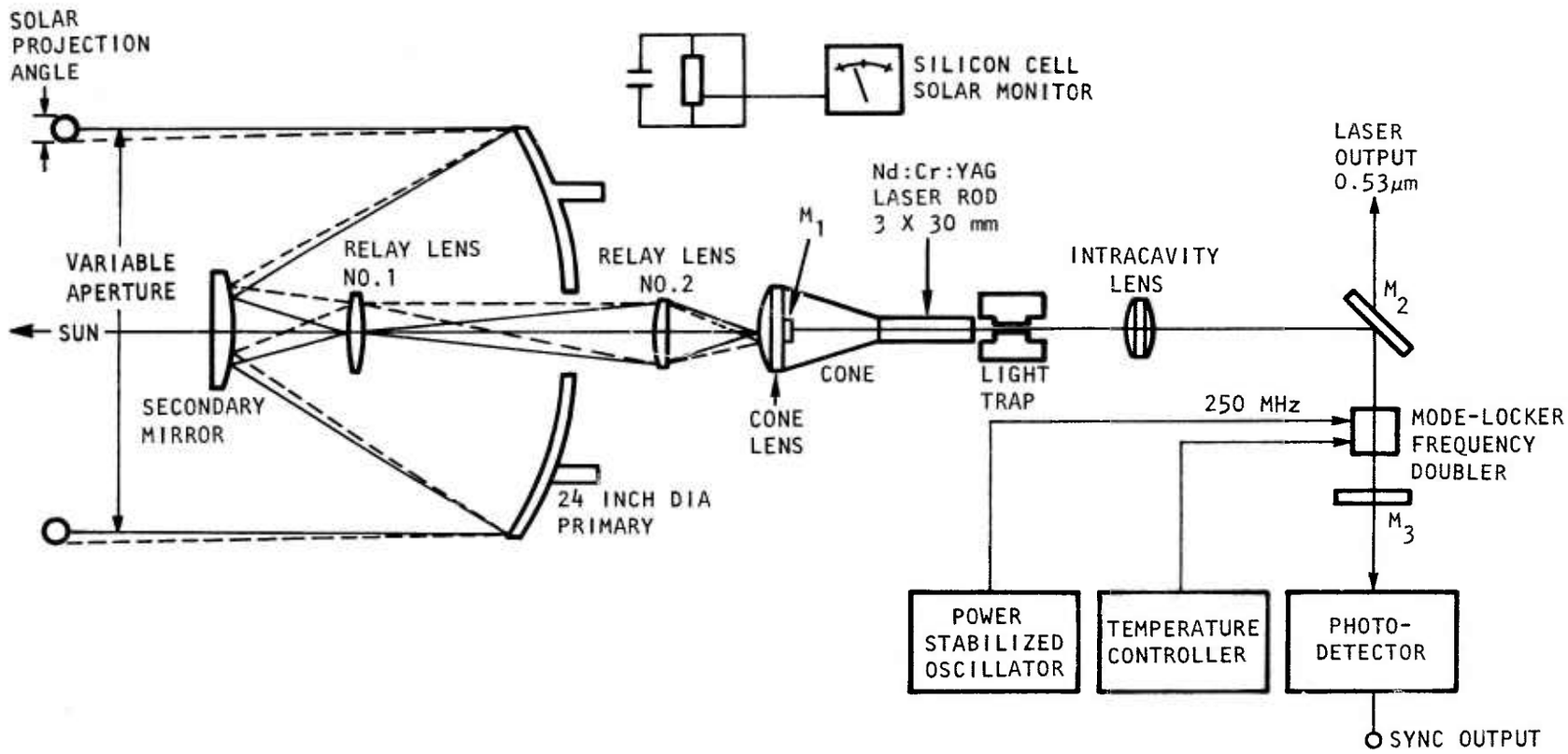

Figure 11 Solar Pumped Laser Schematic

The basic laser resonator shown in Figure 9 is the primary feature in common. The 1.06μm leg of the L cavity contains the HR 1.06μm mirror, the laser rod and the intracavity lens. The mode locking/frequency doubling leg contains the AOML/FD employing the BSN crystal, and the dichroic mirror HR at both 1.06μm and 0.53μm. The legs are joined by the folding mirror which is HR for 1.06μm polarized vertically with respect to the plane of the L, and highly transmissive for the orthogonal polarization of the second harmonic.

The AOML/FD configuration used is the same physically, optically and electronically. All the passive optical elements except the HR 1.06μm mirror are configured the same for both lasers. Laser radiation transmitted through the dichroic mirror is used to provide the optical signal for the clock (sync) output. In both units, the laser rods are canted 0.5^{o} so the planar rod end surfaces are not normal to the beam axis or parallel to each other, thus discouraging etalon interactions between surfaces.

Invar is used for the laser structure, which is very similar to its lamp pumped laser counterpart except for the pumping and cooling section. The AOML/FD mount, the dichroic mirror mount, the folding mirror mount and the clock detector assembly are virtually identical in both lasers.

Both lasers are designed to be purged with dry nitrogen, then operated with the optical path sealed from ambient atmosphere. Heat is removed through cold plates in both units.

3.3 Features Peculiar to the Solar Pumped Laser

Most of the features peculiar to this laser result from the end pumping geometry used in this and several previous solar pumped laser programs. By referring to Figure 11, it can be seen that the pump light must enter the rod through one end, and to do so must pass through or around the 1.06μm HR mirror M_1. To reduce the spot diameter of the pump light, a condensing cone is used between the final lens in the pump optical train and the laser rod. Because of the axial nature of the pump light, the unabsorbed light exiting the laser rod through the end away from the mirror M_1 would heat the entire laser. The light trap prevents this from occurring by absorbing 97% of the throughputted light.

On the previous program, it was found experimentally that a 30 mm long laser rod of standard nominal 1% Nd doping made adequate use of the available pump light. Significantly higher doping would decrease laser rod optical quality and upper laser level lifetime. A longer rod would absorb very little extra pump radiation. Concerning the rod diameter, analysis shows that the smallest diameter possible produces the most power, all other constraints being held constant and provided these are sufficient Nd ions in the smaller rod to provide the inversion necessary. The following mathematical model was used for laser performance:

$$P_{out} = \frac{T}{\beta} \left(\frac{g_o}{\alpha_o + T/2} - 1 \right)$$

where P_{out} is the laser output power, T, the laser output coupling, β, the saturation parameter, α_o, the cavity single pass loss, and g_o, the unsaturated cavity single pass gain. Optimizing transmission for maximum output:

$$(P_{out})_{max} = \frac{2}{\beta} \left(\sqrt{g_o} - \sqrt{\alpha_o} \right)^2$$

$$= \frac{2g_o}{\beta} \left(1 - \sqrt{\frac{\alpha_o}{g_o}} \right)^2$$

Both g_o and β are inversely proportional to rod area so only the $\left(1 - \sqrt{\alpha_o/g_o}\right)^2$ term is area dependent. Thus, the smaller the area, the larger the gain, the larger the output power. The minimum pump light circle which can be obtained is 2.84 mm in diameter[2]. Thus a 3 mm diameter rod was chosen.

The laser rod, condensing cone and light trap are the components which must be cooled. They are placed in close proximity to confine pump source heating effects, and are cooled through a single cold plate. This is discussed in Section 3.4, cold plate subassembly.

The cone lens mount is unique to the solar pumped laser because the lens serves to introduce the pump light to the laser as well as provide the HR 1.06μm mirror. The lens is larger than the mirror, and thus the mount had to

be designed to accommodate this.

The PSQM laser employs a germanium photodiode (TIXL57) as a clock detector, rather than a silicon device (TIXL56) which is used in the EFM lamp pumped laser. The germanium device can be operated at a higher bias current, requiring 26 dB less amplification than the silicon device. In addition, while the phase error for a 2:1 optical power input change for the germanium device is twice that for the silicon device, its random phase noise for a typical input of 1 mW optical power is only 12% that of the silicon device. The phase errors are listed in Table 8. In addition, it was felt the use of the germanium device in the Solar Pumped Laser would provide experimental comparison with the silicon device, which is used in the EFM Lamp Pumped Laser[5].

The laser is mounted on a plate which can be mounted on the solar collector experimental shelf or on a table in conjunction with the solar simulator. A portion of this structure is visible below the PSQM laser in Figure 1. Translation along three orthogonal axes was provided, as well as rotation about a vertical axis passing through the cone lens.

3.4 Cold Plate Subassembly

The condensing cone, laser rod and heat sink, light trap and cold plate form the cold plate subassembly, two view of which are shown in Figure 12. Two cold plates were made for the laser, the one shown here having been configured for cooling with EFM lamp pumped laser heat pipes. The other cold plate, cooled by flowing refrigerated liquid, is shown with cooling lines attached in Figure 1. Both are fabricated from aluminum, and have a black anodized finish. The top of the cold plate, upon which the three components are mounted, has not been anodized but has been carefully machined and smoothed to improve thermal conduction across the interface.

Prior to this PSQM laser, previous solar pumped lasers[1,2,3] employed electroformed silver condensing cones. The electroforming utilized a carefully machined and polished stainless steel mandrel, which limited the optical quality of the conical reflecting surface. In electroforming, the silver layer was electrodeposited on the mandrel. This was followed with a thick copper layer

TABLE 8

TYPICAL PHASE ERRORS FOR CANDIDATE
SILICON AND GERMANIUM CLOCK DETECTORS

	$\Delta\phi$ for 2:1 OPTICAL POWER CHANGE	RANDOM PHASE NOISE for 1 mW $P_{OPTICAL}$	PHASE WITHIN VALUE FOR 99% TIME
Ge DETECTOR	4°	0.081° rms	0.45°
Si DETECTOR	2°	0.7° rms	3.5°

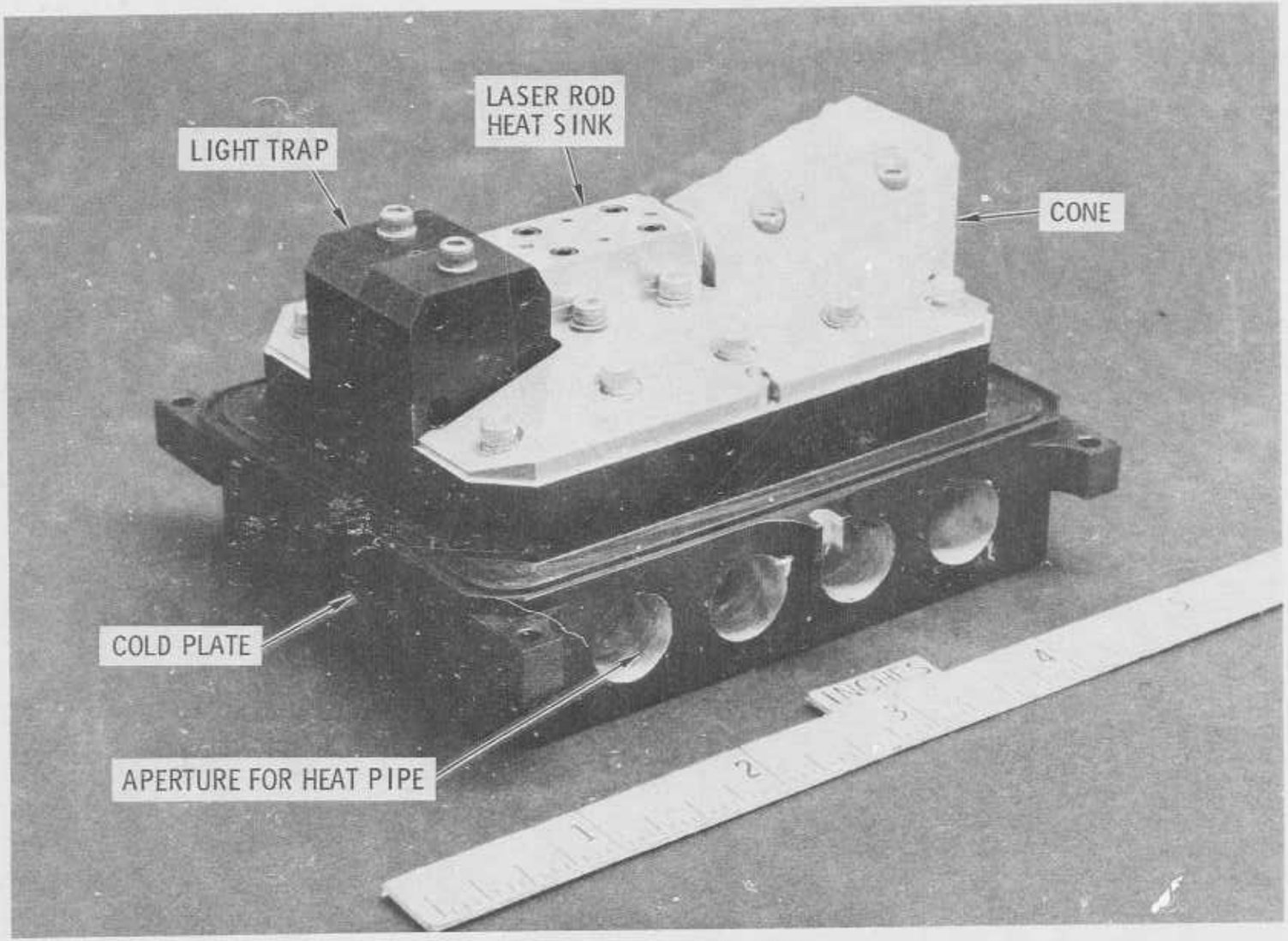

Figure 12(a) Cold Plate Assembly

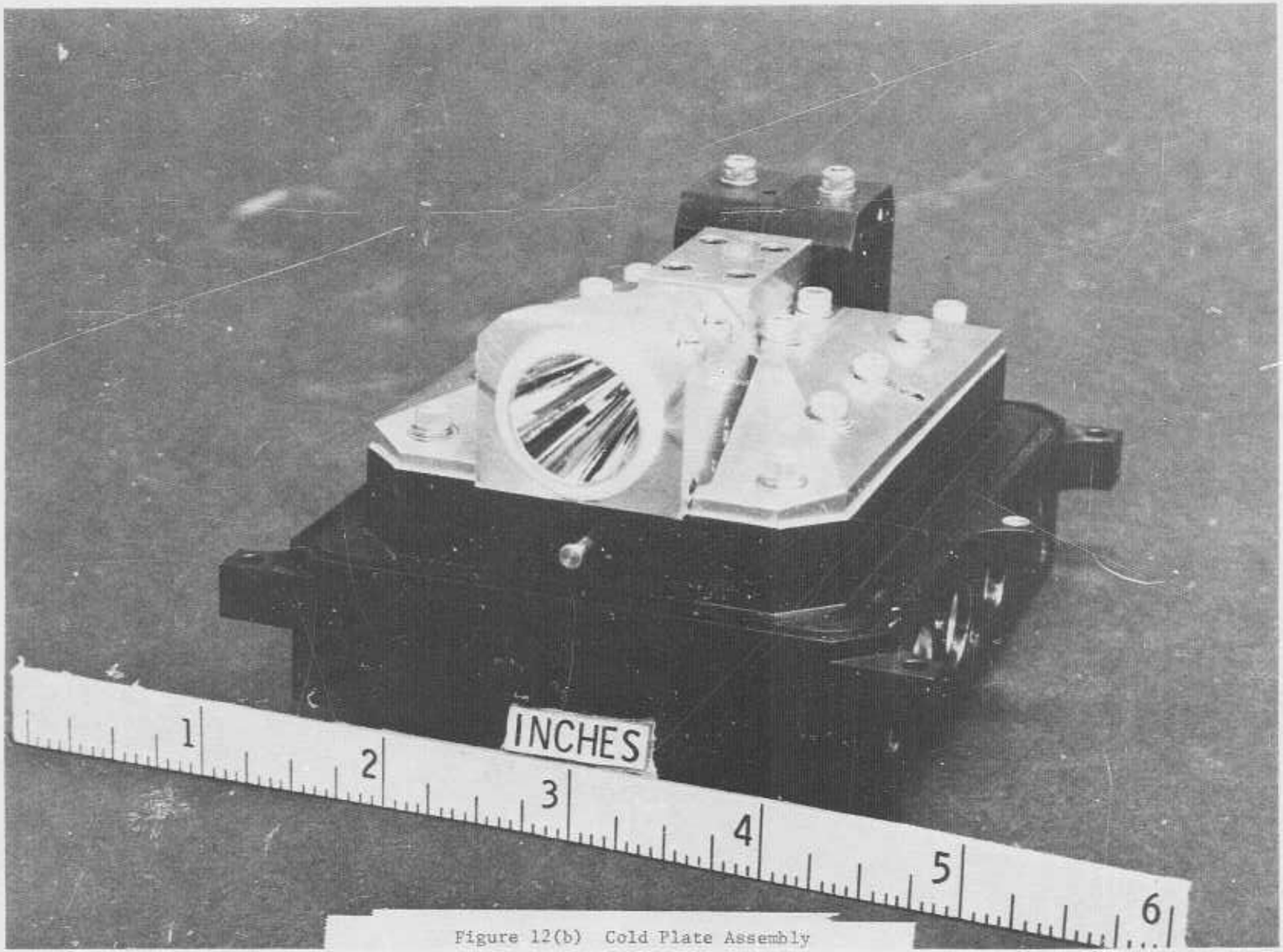

Figure 12(b) Cold Plate Assembly

for strength and good thermal conduction. The silver eventually tarnished, decreasing light throughput.

The cone used in this although identical in optical design to those used on previous programs[1,2,3] laser was replicated on a high optical quality glass mandrel. The technique is more difficult and expensive, but the high quality of the reflecting surface is readily apparent to the eye. The cone structure (not including the replicated portion) is made of aluminum. Figure 12b shows the entrance end of the cone. The structure is fabricated in four closely fitting sections, employing guide pins to maintain tolerance. A replicated surface is formed on the mandrel surface,epoxied to one of the quarter sections, then thermally shocked free of the mandrel. The assembled cone structure is located with respect to the laser rod heat sink with a guide pin in the heat sink. This assures horizontal centering of the rod in the small end of the cone and protects the protruding portion of the rod from damage during assembly and disassembly. Since little heat (10-20 watts) is absorbed in the cone, the contact area to the cold plate is not large ($\sim$0.9 square inches) and four bolts suffice to hold the cone structure in adequate thermal contact with the cold plate.

The laser rod heat sink is machined from copper and is essentially the same as the heat sink used on the previous laser. The contact area is large, approximately 6 square inches, to cool the laser rod as much as possible. Fourteen bolts tie the heat sink to the cold plate, positioning being fixed by two guide pins in the cold plate. The surface which contacts the cold plate is carefully machined and smoothed to improve thermal conduction.

The light trap is black anodized aluminum. It contains a clear aperture for the laser beam and a series of baffles inside to absorb most of the pump source light exiting the laser rod. This light is not collimated, so the baffle arrangement does remove most of it from the resonator. The light trap is located with respect to the rod heat sink with a guide pin in the heat sink, just as the cone is.

The laser rod heat sink is first bolted in place. The cone and light trap are then positioned by their guide pins and bolted in place. The three components have machined holes in their top surfaces to allow thermocouples to be inserted and cemented in place. The cone temperature is measured near the small end very close to the end of the laser rod. The laser rod heat sink has two thermocouple holes, one above each end of the rod. The light trap has a hole for this purpose in its top surface.

3.5 Mirror Mounts and AOML/FD Mount

The mounts are described briefly in this section, since much of the design work was performed during the EFM lamp pumped laser program. The design and description of the mounts are covered more fully in the report of that program[5].

The dichroic mirror mount, which holds mirror M_3 in Figure 11, is shown in Figure 13. Figure 13a is a view of the dichroic mirror mount from the adjustment side, the side away from the laser resonator. The knurled adjustment knobs are removable, after the locking clips are locked. The central hole shown in the figure holds the mirror assembly which directs the laser light transmitted through the dichroic mirror to the clock detector. The central hole in Figure 13b, showing the resonator side of the mirror mount, holds the dichroic mirror. The mount is made primarily of beryllium copper. The flexural pivots are twisted after machining, then heat treated, to bias them to provide the torsional force which allows the adjustment knobs to function. The mount providing two axis rotation of the dichroic mirror, M_3, about the mirror center. Cavity length is grossly adjustable by shimming the dichroic mirror mount, fine adjustment being provided by a translation stage attachable to the cone lens mount.

The cone lens holder is shown in Figure 14. This holder is unique to the solar pumped laser, since the cone lens allows throughput of pump light as well as containing the HR 1.06μm mirror. Thus, the optical element, the lens, is much larger than the corresponding mirror of the EFM lamp pumped laser. The structure is fabricated primarily from aluminum, with beryllium copper locking clips and Bendix Flexural Pivots. The adjustment knobs on the side away from the resonator (Figure 14a) are removable, as are those of the dichroic mirror mount. A short bellows mates to the central section on the resonator side of the mount (Figure 14b) to seal the optical path between the mirror on the cone lens and the laser

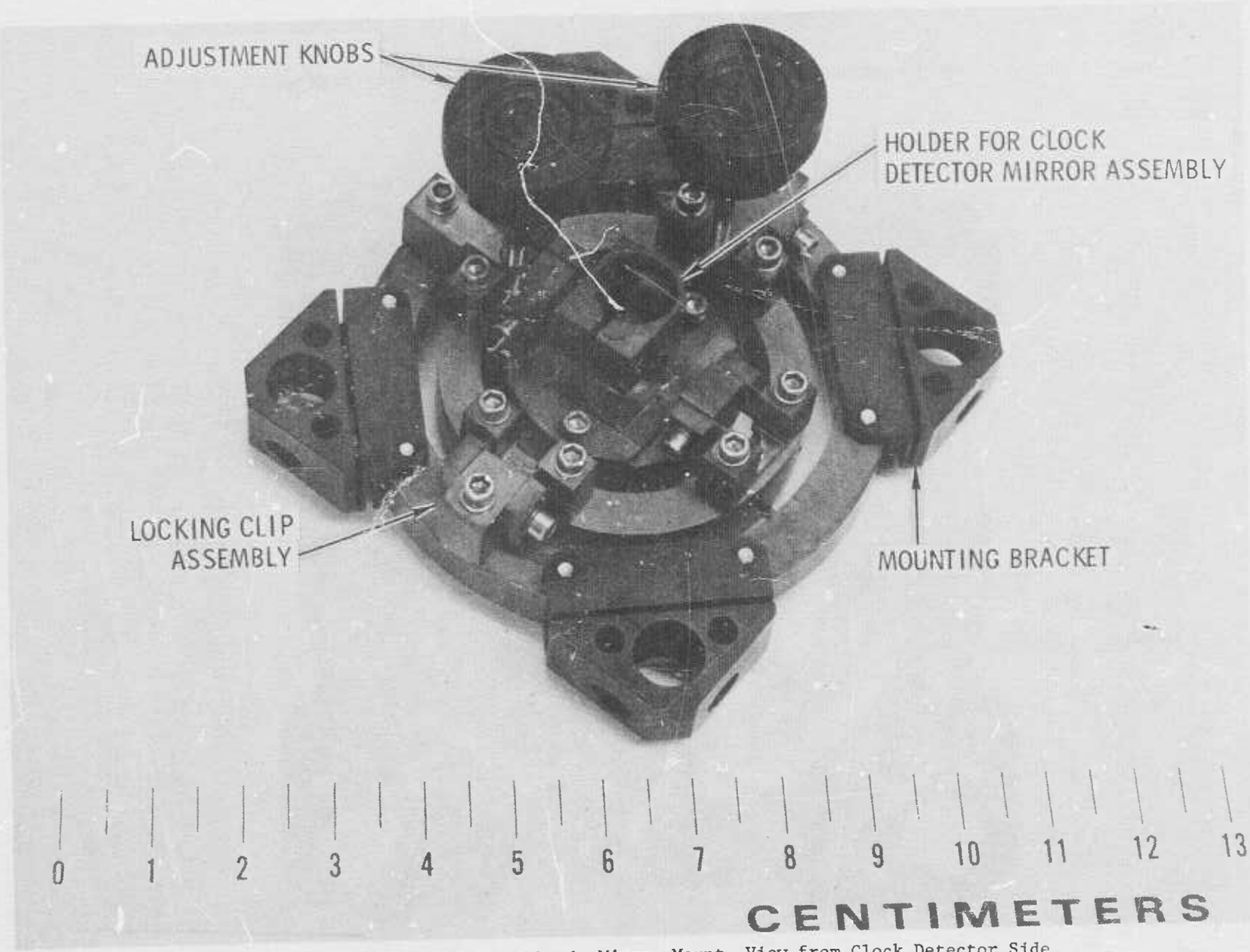

Figure 13(a) Dichroic Mirror Mount, View from Clock Detector Side

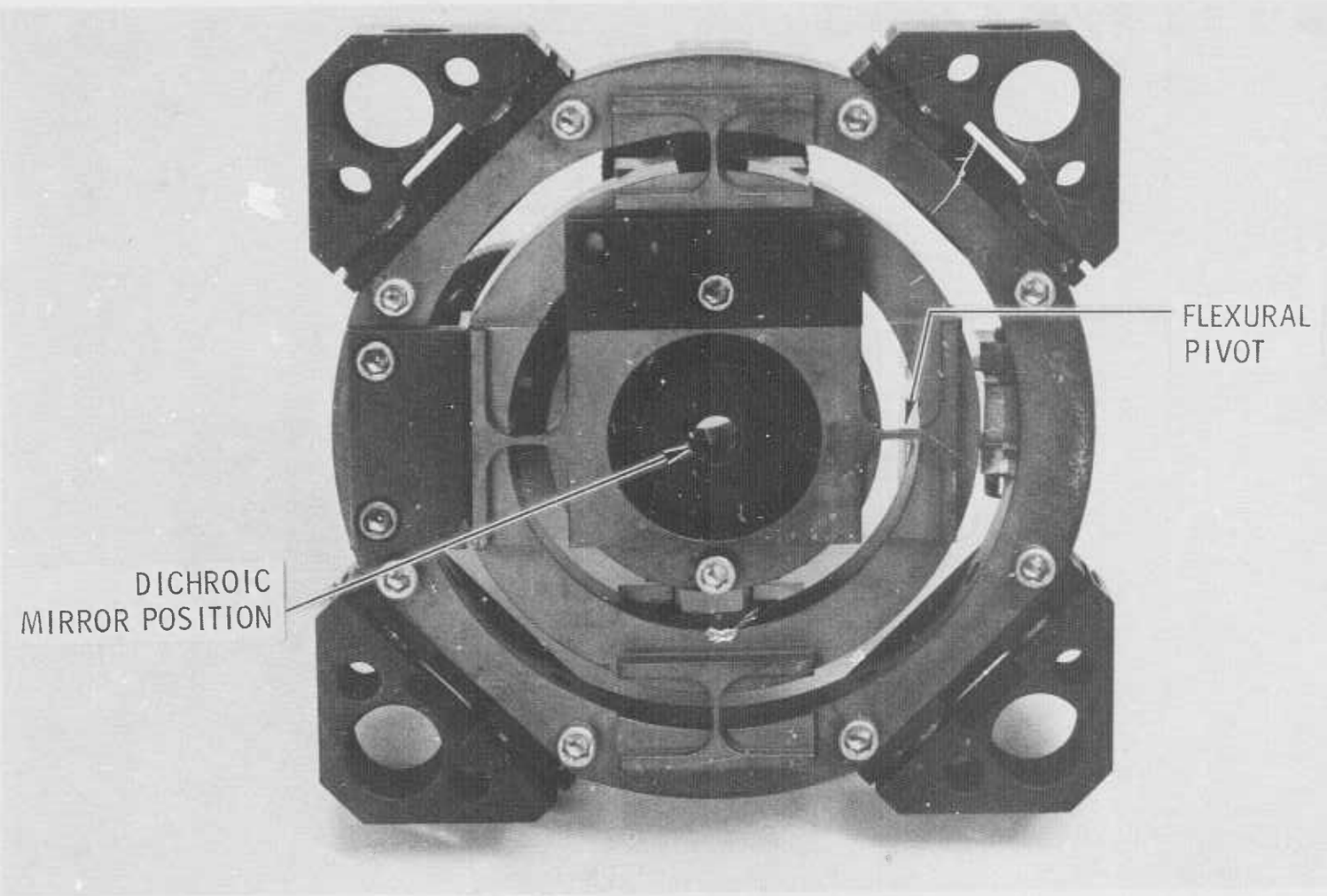

Figure 13(b) Dichroic Mirror Mount, View from Resonator Side

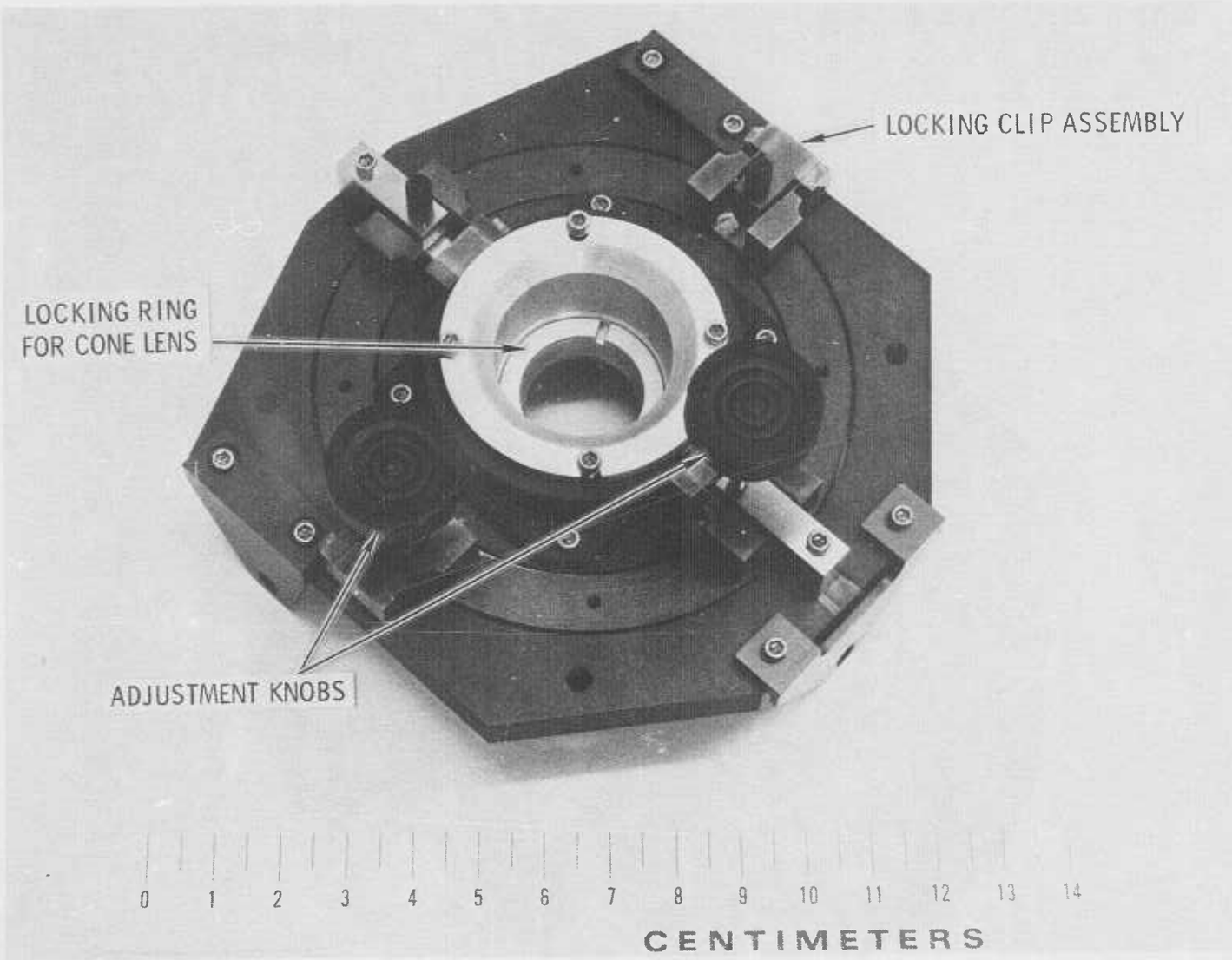

Figure 14(a) Cone Lens Mount, View from Pump Light Input Side

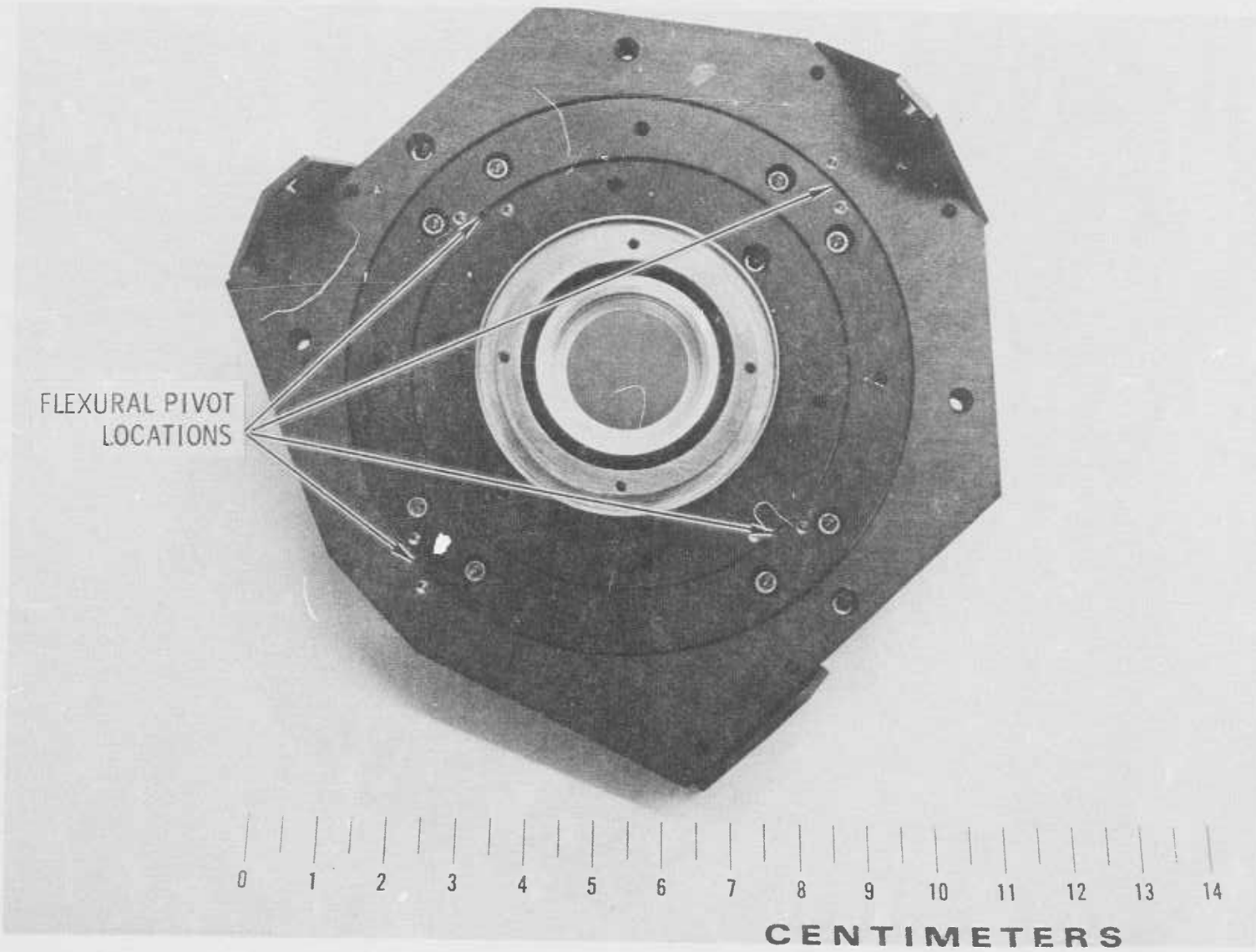

Figure 14(b) Cone Lens Mount, View from Resonator Side

structure opening at the cone. A translation stage is mounted to the laser structure, to position the cone lens holder for resonator cavity length adjustment. The stage, shown in Figure 17(a) later in this report, is removed after the mount provides two axis rotation about the cone lens, which also contains the flat HR 1.06μm mirror, M_1.

The AOML/FD mount is shown in Figure 15. Fabricated primarily from aluminum, the mount is virtually identical to the one on the EFM lamp pumped laser[5]. The 250 MHz RF drive signal is introduced to the AOML/FD unit through the OSM connector. Four feedthrough connections allow the crystal oven for frequency doubling to be temperature controlled and monitored. The unit can be rotated within the mount for Bragg angle adjustment for mode locking. The mount can be adjusted normal to the laser beam axis with a translation stage, shown in Figure 17(a). This allows the beam to pass through the portion of the BSN crystal which produces optimal mode locking and frequency doubling. The stage is removed after positipning of the AOML/FD and its mount.

3.6 Laser Structure

The laser structure is shown in Figure 16. It is machined from a solid block of invar measuring approximately 6 x 6 x 12 inches. The invar is heat treated twice during the fabrication to allow the alloy to relax to its normally low expansion coefficient state. The structure is rhodium plated for a hard, attractive finish, and weighs approximately 7-1/4 pounds.

The heat sink subassembly shown in Figure 12 fits upside down into the compartment indicated. The intracavity lens is bonded with Duco cement for easy replacement to a mount which slides in its channel, the mount being clamped in the desired position. The folding mirror is held in place with a spring loaded mount in the small compartment indicated.

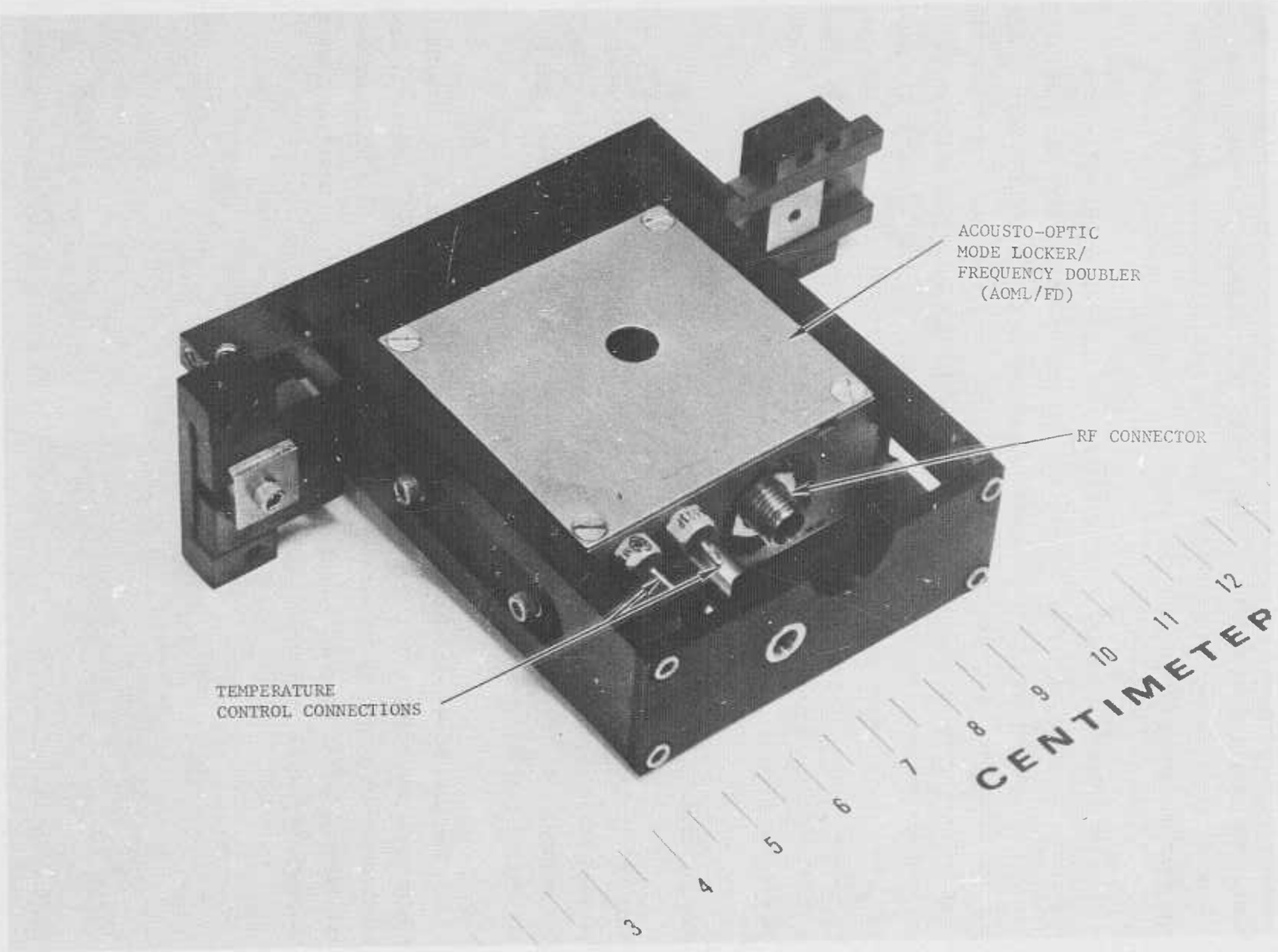

Figure 15 AOML/FD Mount

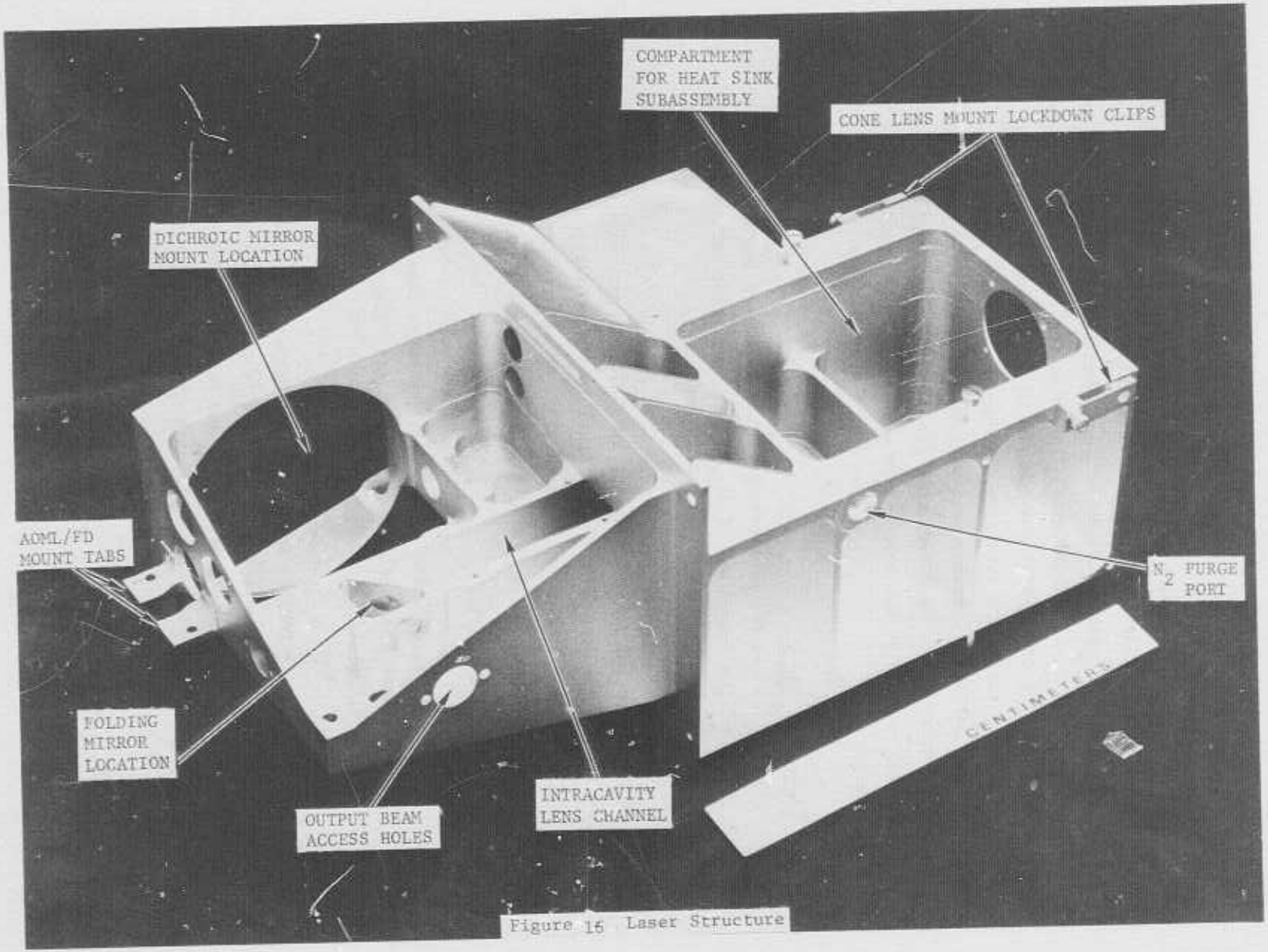

Figure 16 Laser Structure

All laser components mount directly or indirectly to the structure. Provisions are made for attaching the two removable translation stages, one for resonator cavity length adjustment accomplished by translating the cone lens mount along the laser optical axis, the other for optimizing laser performance by laterally translating the AOML/FD in its mount. An enclosure fits over the left hand end of the structure, isolating the laser from outside environment. The enclosure contains exit windows for the 0.53μm output beam and for a 1.06μm monitor beam. The heat sink subassembly compartment is sealed by the subassembly itself at the top, and by a bellows attached to the cone lens mount at the end.

3.7 Assembled Laser

Figure 17 shows two photographs of the assembled laser. The view shown in Figure 17a is of the output end of the laser. The input end is shown in Figure 17b.

The translation stage for cavity length adjustment is attached to the laser structure and the cone lens mount. Prior to its removal, the cone lens mount is locked in place. Similarly, the AOML/FD translation stage is attached to the structure and the AOML/FD mount, and a similar procedure is used for its removal.

The cold plate, on which are mounted the cone, laser rod heat sink, and light trap, is shown inverted, the three elements being in the compartment below. The heat pipe cold plate is shown.

The intracavity lens is mounted in its holder in the channel shown in Figure 16. Here the holder is fixed in position by a cover plate. Similarly, the folding mirror is mounted in its compartment and held in position by its cover plate. Between the folding mirror and the AOML/FD unit there is a sealed dust tube to keep the laser beam path clear and to protect surfaces from contamination. Also

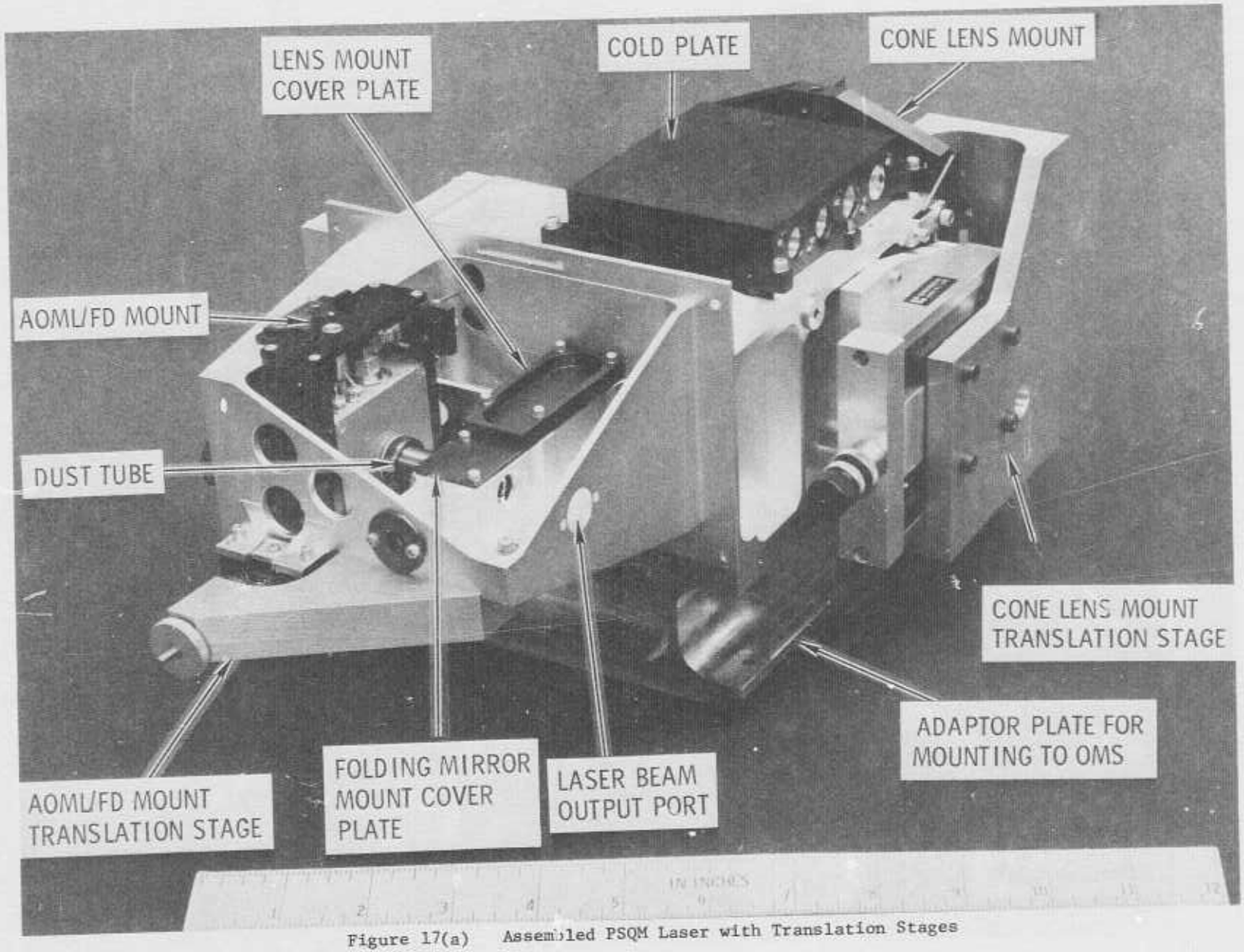

Figure 17(a) Assembled PSQM Laser with Translation Stages

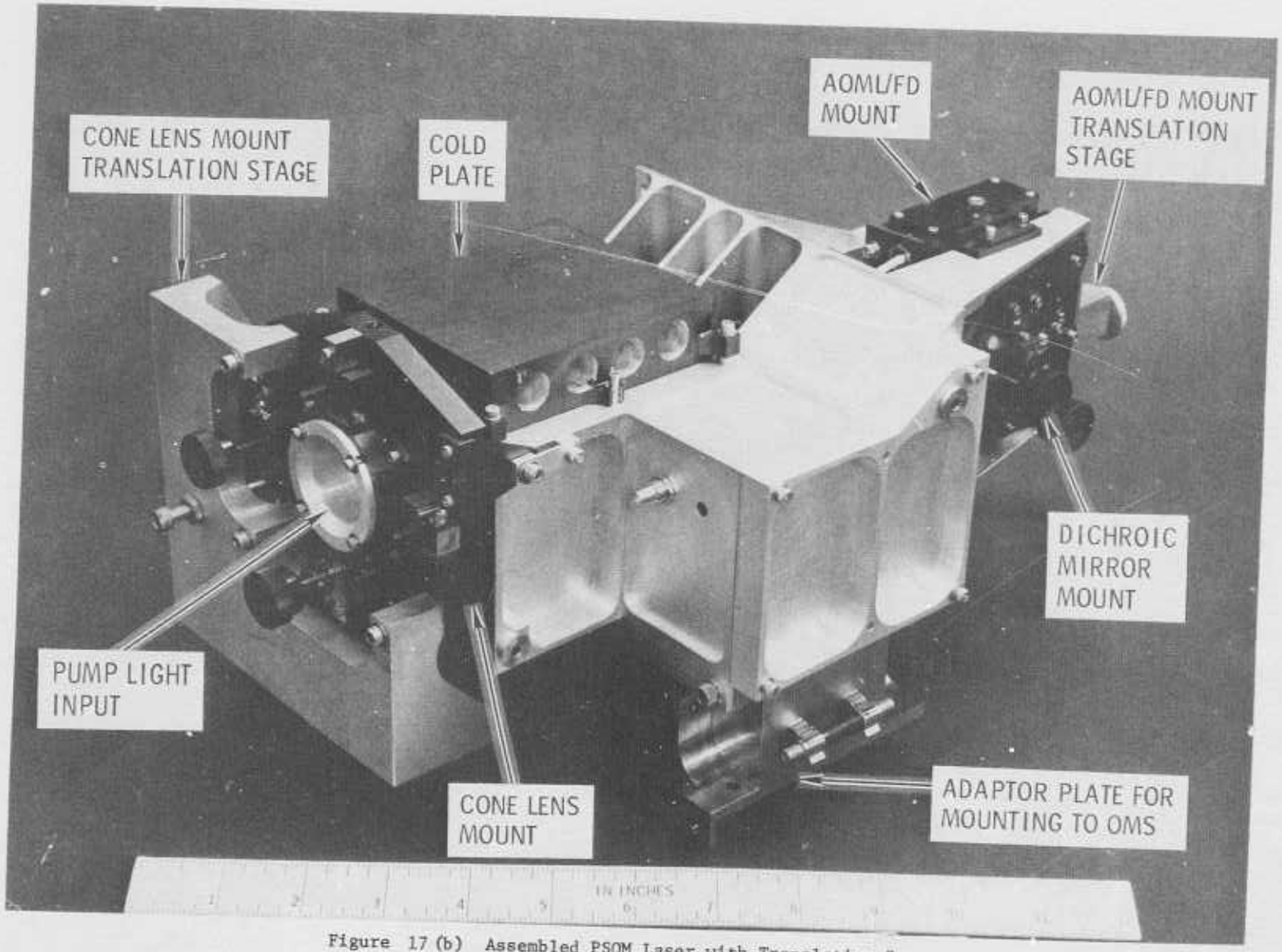

Figure 17 (b) Assembled PSQM Laser with Translation Stages

for beam path protection, there is a bellows between the dichroic mirror mount and the AOML/FD, and another between the cone lens mount and the cold plate subassembly compartment. The folding mirror mount seals the path between the AOML/FD and the intracavity lens, the lens also serving to seal the cold plate subassembly compartment.

Figure 18 shows the laser from the front with the translation stages removed. Figure 19 shows the laser from the output end with the enclosure in place. The enclosure has two windows, one for the mode locked, frequency doubled output beam, the other for monitoring the 1.06μm performance.

3.8 Electronics

Virtually no electronics development was performed on this program, having been completed previously on the EFM lamp pumped laser program and discussed in the final report[5]. A short description only is included here.

The laser electronics consists of five functional units, located within the laser and in three external packages. The functional units are:

1. AOML/FD drive control
2. AOML/FD oven control
3. Clock electronics
4. Laser monitor
5. Power supply

The three external packages are the AOML/FD Control which includes 1. and 2. above; the Monitor, which corresponds to 4. above and includes monitoring of 1. and 2. and 3; and the Power Supply which provides d.c. power to the AOML/FD Control.

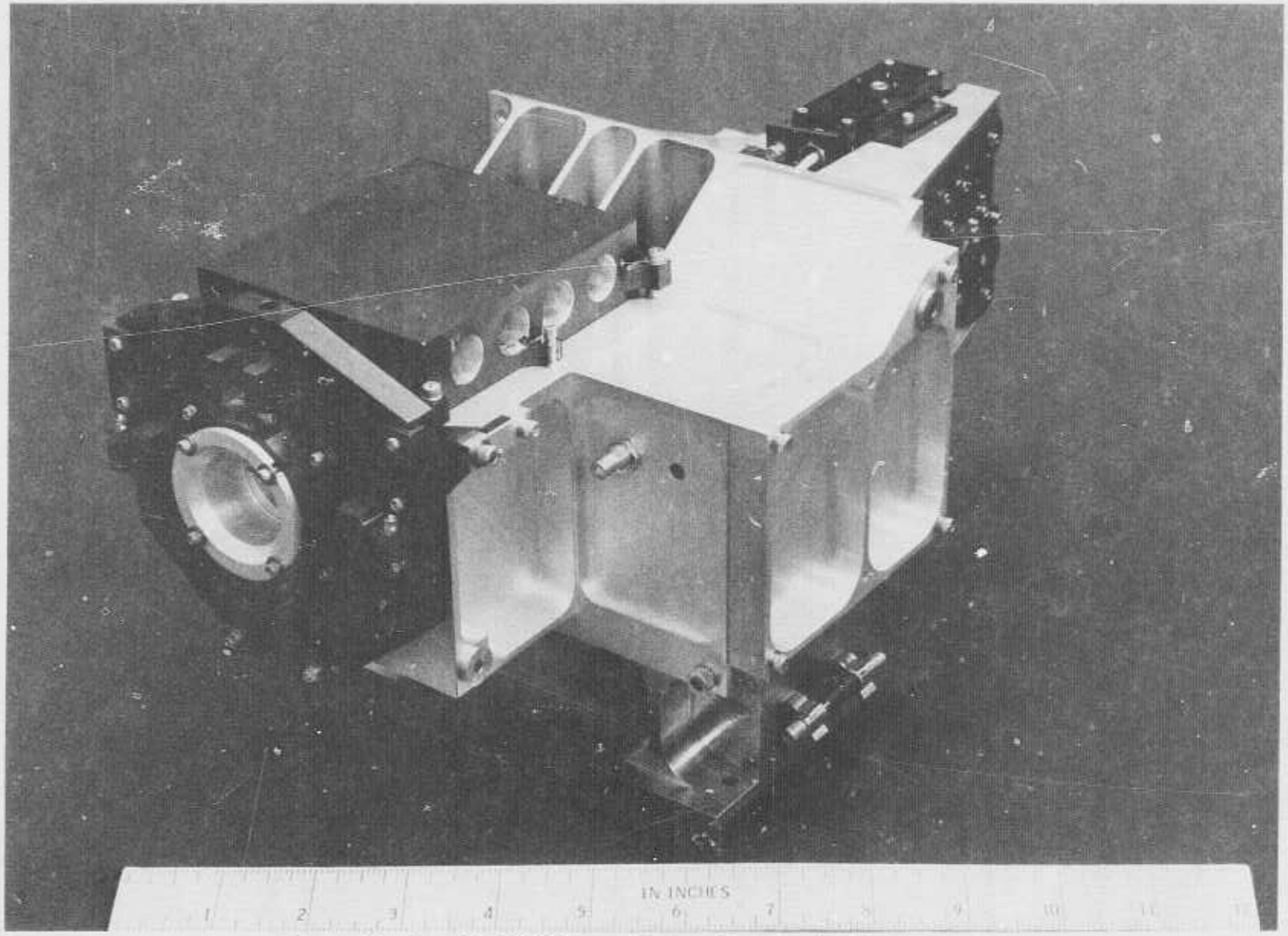

Figure 18 Assembled PSQM Laser Without Translation Stages

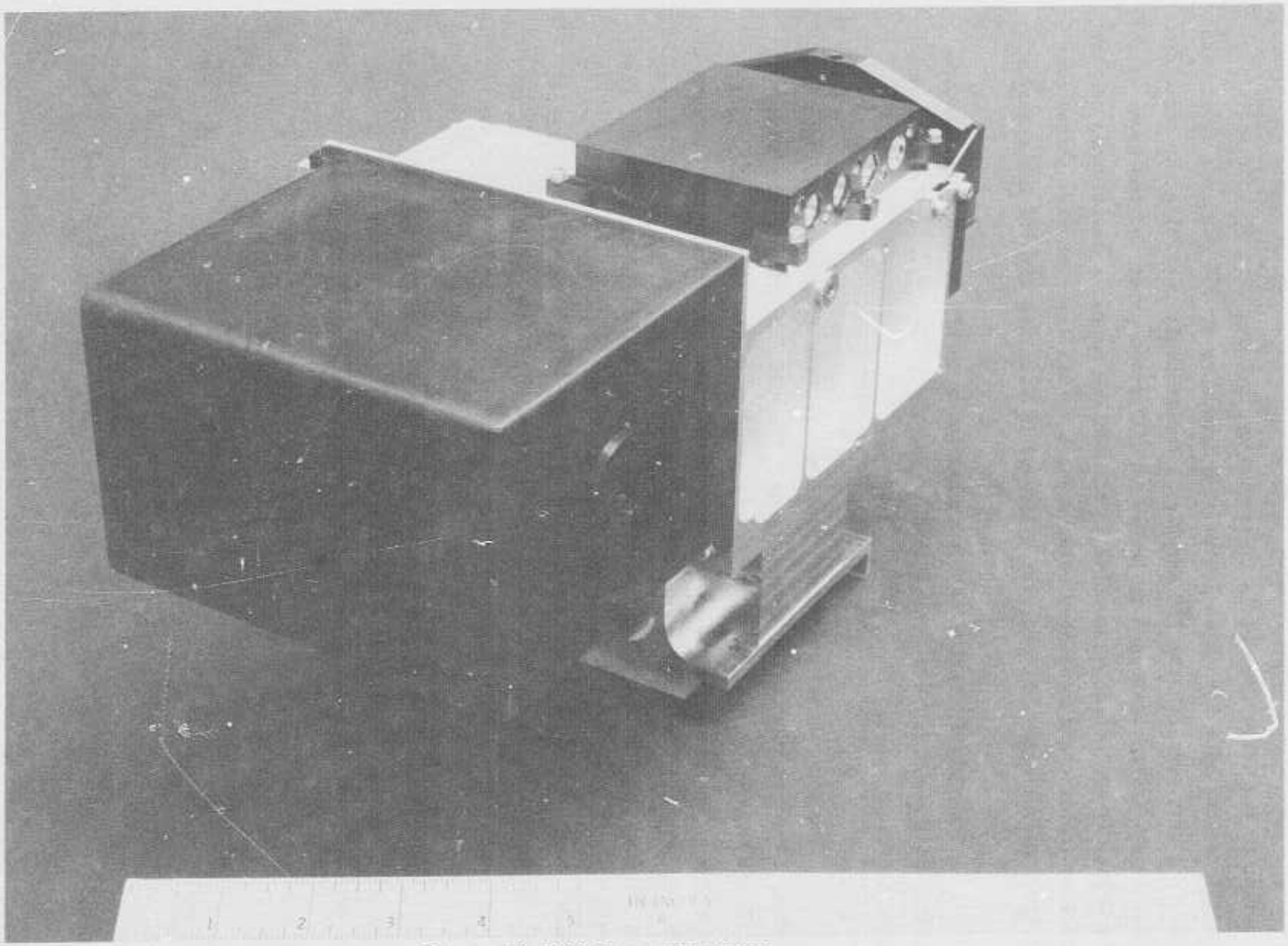

Figure 19 PSQM Laser with Cover

The AOML/FD drive control block diagram is shown in Figure 20. The function of the drive control is to provide up to 5 watts of RF power to drive the BSN crystal as a loss mode locker at a frequency of 250 MHz, and to provide a 500 MHz sync signal. The 250 MHz signal amplitude is controlled by circuitry whose inputs are incident and reflected AOML/FD drive power and the level set. The signal is amplified and coupled to the AOML/FD unit. A directional coupler provides incident and reflected power signals, which input to the control circuitry. A sync output is provided by frequency doubling the 250 MHz signal.

The AOML/FD Control also provides drive to and feedback temperature control of the AOML/FD oven for frequency doubling. The oven drive set control is on the front panel.

The Monitor has two front panel meters, one to display voltages and powers, the other to display temperatures. The AOML/FD Control and Monitor units are shown in Figure 21. It must be noted that the units in this photograph are actually EFM lamp pumped laser units. The AOML/FD control is identical for both lasers. The solar pumped laser Monitor differs from its EFM counterpart in that the Cathode Holder temperature meter is not present, and the test points for the temperature meter are Rod Heat Sink Top, Cone, Light Trap, and AOML/FD oven. These test points are listed in Table 9. For both electrical and thermal readouts, the test point is selected with its corresponding push button switch.

The clock electronics consist primarily of a TIXL57 germanium photodiode and two stage amplifier. All electronics are in the laser itself. The bias supply comes from the power supply through the AOML/FD Control.

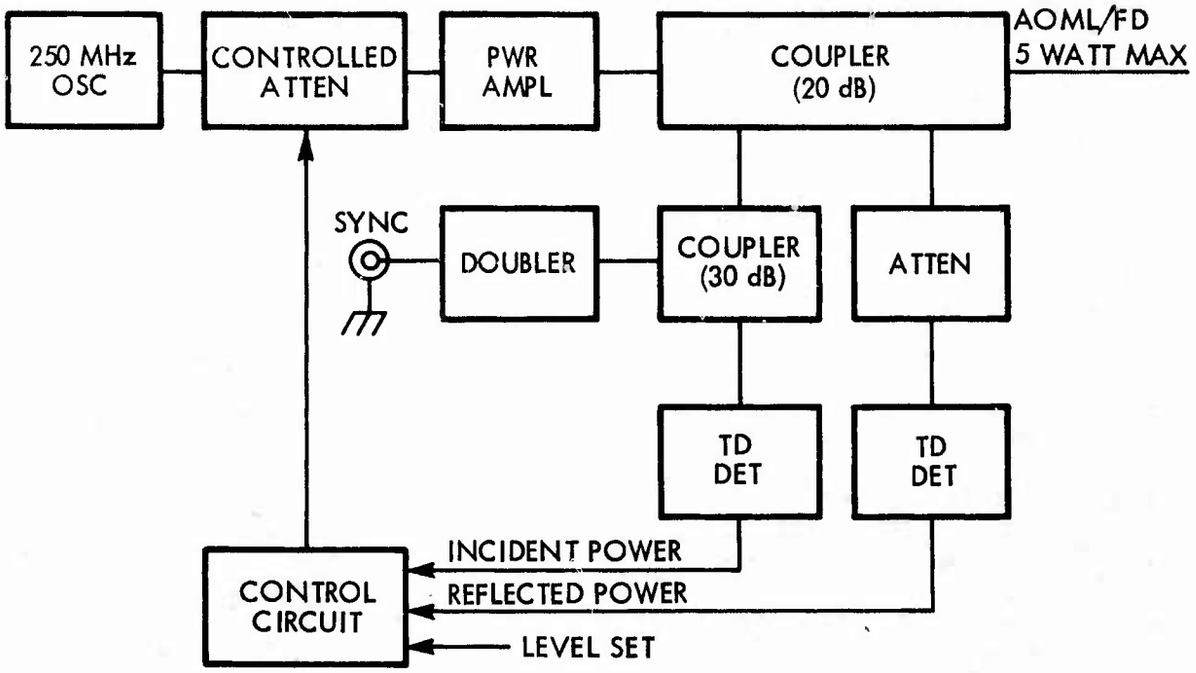

Figure 20 AOML/FD Drive Block Diagram

Figure 21 Electronics Panels

Table 9

SOLAR PUMPED LASER TEST POINTS

DISPLAYED ON MONITOR

ELECTRICAL

AOML/FD OVEN ERROR

AOML/FD HEATER VOLTAGE

DETECTOR DIODE BIAS

RF INCIDENT POWER

RF REFLECTED POWER

THERMAL

ROD HEAT SINK TOP TEMPERATURE

CONDENSING CONE TEMPERATURE

LIGHT TRAP TEMPERATURE

AOML/FD OVEN TEMPERATURE

Section IV

LASER TESTING

4.1 Introduction

The solar telescope as configured for use with the solar pumped laser is described in Section 4.2.

Testing results with the developmental laser and the PSQM laser, prior to the testing covered by the General Test Plan, is presented in Section 4.3. These results include a comparison of laser multimode output power with the various secondary mirrors for Nd and Nd:Cr doped YAG rods. Mode locked, frequency doubled results are presented also.

General Test Plan testing results are presented in Section 4.4. These results were obtained with the 405B Project Engineer present.

Test performed subsequent to those discussed in the previous section a presented and discussed in Section 4.5.

4.2 Laser Operation with the Solar Telescope

While the solar simulator was used for alignment of the PSQM las for preliminary testing, the solar telescope was used for all quantitative ts reported in this section.

The telescope optical schematic is shown in Figure 11. The telescope optical elements and positions are described in Table 10. The primary mirror was recoated prior to its use on this program, the coating being vacuum deposited, dielectrically overcoated silver. The coating was protected, prior to first usage, by a sprayed on vinyl film, which is easily peeled from the mirror. Application and subsequent removal of such a film is a good method of removing dust from the primary mirror.

Table 10

SOLAR TELESCOPE ELEMENTS AND POSITIONS

Element	Description	Position
Primary Mirror	24" diameter paraboloid Focal length = 35.74"	Reference
Secondary Mirror	3" or 2-1/2" diameter spherical Focal length = 3.51"	33" from primary (above)
Relay Lens No. 1 (Field Lens)	3" diameter equiconvex, spherical Quartz Focal length = 10.6" Antireflection Coated	12" from primary (above)
Relay Lens No. 2 (Final Lens)	3" diameter Plano-convex, spherical Glass Focal length = 4.0" Antireflection Coated	7" from primary (below)

Five secondary mirrors are or were available for use with the telescope. Their properties are summarized in Table 11. The first four were available from the last program, the fifth having been obtained near the end of this program. The dielectric mirrors were used to selectively reflect the useable pump light to the laser rod while transmitting as much as possible of the unwanted portions of the spectrum on both sides of the pump bands. The old narrow band dielectric secondary, number four in Table 11, was fabricated in 1971, and it was felt that a better replacement should be obtained (number five in the table). The replacement was received too late in the program to be used.

The 3" diameter silver secondary mirror coating had degraded over a portion of the reflecting surface. The visible degradation appeared to have been caused by the presence of a contaminant such as finger oil, which was burned into the mirror coating by the concentrated sunlight from the 24" primary mirror. Removal of the silver for subsequent recoating of the substrate revealed most of the glass surface to be etched. The removal was accomplished with nitric acid, HNO_3, which does not attack glass. The etching apparently was caused by prolonged action of the concentrated sunlight on the overcoated silver.

The purpose of the wideband dielectric mirror, number three, is to reflect pump light for both Nd and Cr excitation. The narrow band dielectric mirrors are for Nd excitation.

Testing of the three mirrors available for use at the time, numbers one, three and four, showed their reflective properties to be unchanged from previous measurements. Spectra of the two dielectric secondary mirrors used appeared in previous reports[2,3].

Solar intensity was monitored with a silicon solar cell detector connected to a milliameter. This was not calibrated absolutely, but provided relative solar intensity measurements. The solar cell is mounted in an aluminum box with its field of view apertured to about 5^{o}. Two neutral density filters prevent saturation of the detector and provide electrical output compatible with the meter. A reading of 7.4 (0.74 of full scale) was the best ever recorded while operating at Sylvania. Readings of greater than 7.0 occasionally were obtained, while readings greater than 6.5 were common.

Table 11

SOLAR TELESCOPE SECONDARY MIRRORS

Mirror	Diameter	High Reflectivity Band (μm)	Comments
Silver	2-1/2"	Wideband	-
Silver	3"	Wideband	Discolored, substrate pitted
Dielectric	3"	0.43 - 0.88	Designed for Nd:Cr[3]
Dielectric	3"	0.645 - 0.88	Original dielectric[2] mirror, designed for Nd only
Dielectric	3"	0.72 - 0.90	Designed for Nd only New, obtained too late for use on this program.

Because of the high gain of the laser rod end pumped by the sun, it was difficult to suppress higher order modes on days when sun intensity was high. Suppression was obtained by moving the intracavity lens to force the beam size in the laser rod to be large enough to cause significant losses to the higher order modes. This also increases loss to the TEM_{oo} mode. Thus, an increase in gain caused by increased pump light intensity does not increase TEM_{oo} mode power in any simple manner. Aperturing at any point in the cavity will not improve the situation, since the relative radial energy distribution of all the modes is constant.

In operating the solar pumped laser at sea level, the atmosphere plays a role. The primary loss mechanism for pump radiation is scattering, which depends on thickness of the atmosphere traversed by the sunlight, dust, haze and wispy clouds. The solar monitor seemed to provide an accurate measure of pump light in the presence of scattering from these sources.

Variation in solar intensity while operating the laser produce relatively unstable operation. Sudden or even gradual pump power increases or decreases change the gain of the laser rod and the laser rod focal length. Changes in these produce changes in 1.06μm circulating powers, which produce changes in 0.53μm generated power. This, in turn, affects the temperature of the BSN crystal, which further affects mode locking and frequency doubling, especially since both functions are performed in one crystal.

In addition, dust was blown onto the convex surface of the first cone lens used. The concentrated pump light heated the dust on the lens surface, pitting the broad band antireflection coating and the lens surface itself. This degraded performance of the laser, necessitating the replacement of the cone lens and the aluminum foil dust shield shown in Figure 1.

4.3 Initial Testing

The developmental laser was operated multimode with laser rod 4-27A and 931, both solar pumped, to determine if the telescope/developmental laser combination had degraded. This concern resulted from the inconsistent and relatively poor simulator pumped results discussed in Section 2.2. The results of this testing are summarized in Table 12. Considering the difference in solar monitor reading, the results with rod 931 for this and the previous program are comparable. Thus, the

telescope/developmental laser has not degraded. The highest output powers both with a Nd:YAG and a Nd:Cr:YAG rod were produced with the wideband dielectric mirror.

The developmental laser was operated cw at 1.06μm and a cw at 0.53μm, with Nd:YAG rod 4-27A. The results are summarized in Table 13. The resonator cavity was folded, with AOML/FD D-12 in the cavity as a loss element for 1.06μm tests and for frequency doubling to obtain green output. No mode locking was performed. While the 0.7W at 1.06μm was less than the 0.8W reported on the last program, the 0.53 watts at 0.53um is higher than the 0.43 watts previously obtained. The lower 1.06μm power reported on this program may be due to taking insufficient precautions to ensure TEM_{oo} mode operation previously. Using an infrared phosphor card, a small circular spot is often taken to indicate the TEM_{oo} mode. However, a frequency spectrum often shows other modes to be present. For TEM_{oo} mode results on this program, both the infrared phosphor card image and the spectrum analyzer output indicated TEM_{oo} mode. The higher 0.53μm power on this program is attributed to a different BSN crystal and tighter focussing in the BSN crystal.

The PSQM laser was operated with the best available Nd:YAG (4-27A) and Nd:Cr:YAG (107) rods (see Section 2.4.1). AOML/FD D-20, the unit designed for use in the PSQM laser, was used, with 1.5 watts RF drive. The dichroic mirror had a 2.5 cm radius of curvature; the intracavity lens had a 10 cm focal length. After initial operation and troubleshooting, stable, mode locked, frequency doubled operation was obtained with both rods. The best results obtained are summarized in Table 14. The first entry for each rod indicates the highest power obtained within the 300 psec pulse duration specification. The second entry indicates the highest obtained with longer pulses.

Table 12

Solar Pumped Multimode Performance* of the Pumped Developmental Laser for Two Laser Rods

Laser Rod	Secondary Mirror**	Solar Monitor	Rod Temperature	Multimode Power
*** 931 (Nd:Cr)	Silver	7.2	-	5.1W
931 (Nd:Cr)	Silver	6.6	10°C	4.8W
931 (Nd:Cr)	Wide dielectric	6.65	4°C	5.25W
931 (Nd:Cr)	Narrow dielectric	6.65	-	3.75W
4-27A (Nd)	Silver	6.7	6°C	3.38W
4-27A (Nd)	Wide dielectric	6.85	6°C	3.6W
4-27A (Nd)	Narrow dielectric	6.7	-	2.5W

*Resonator cavity used a 2.5% transmitting, 60 cm mirror
**See Table 11
*** Previous program results (3)

Table 13

Solar Pumped TEM_{oo} Mode Performance of the Developmental Laser, Using Laser Rod 4-27A

Intracavity Lens Focal Length (cm)	Dichroic Mirror Radius of Curvature (cm)	Mirror Transmission (%)	Solar Monitor Reading	Wavelength (μm)	Power (W)
13	5	.042	6.5	1.06	.044
13	5	1.9	6.5	1.06	.630
13	5	2.1	6.05	1.06	.630
13	5	2.5	6.45	1.06	.608
13	5	3.0	6.4	1.06	.700
13	5	-	6.95	.53	.400
13	4	-	7.05	.53	.530

Table 14

Solar Pumped PSQM Laser Mode Locked, Frequency Doubled Performance

Laser Rod	Power (W)	Pulse Duration (psec)	Solar Reading
4-27A (Nd:YAG)	.250	280	6.7
4-27A (Nd:YAG)	.360	420	6.7
107 (Nd:Cr:YAG)	.400	280	6.7
107 (Nd:Cr:YAG)	.480	560	7.0

4.4 Test Results

The results of the tests enumerated and described in the General Test Plan, a document submitted separately during this program, are discussed in this section. The specific tests are listed in Table 15.

For these tests, the laser was operated with Nd:Cr:YAG laser rod 107, a 10 cm focal length equiconvex intracavity lens, a 2.5 radius of curvature dichroic mirror, and AOML/FD D-20. The telescope was equipped with the wideband dielectric secondary mirror. The refrigerated coolant cold plate (see Figure 1) was used. The laser was purged with dry nitrogen gas, and the beam path sealed.

4.4.1 Tests 1-5, Interfacing

The laser was mounted on a plate which allowed it to be operated with the solar telescope (tests 1 and 4) and the solar simulator (tests 2 and 5). The laser was operated with both sources, satisfying these four tests.

The laser was designed with an interface plate to allow mounting directly to the EFM lamp pumped laser opto-mechanical structure (OMS). The OMS was not available for interface testing, so test 3 was satisfied by comparing the laser interface dimensions to those on the OMS Assembly Drawing.

4.4.2 Test 6, Wavelength

Wavelengths of the laser output are inherent properties of the Nd:YAG laser and the frequency doubling crystal. No detailed testing of the wavelength was performed. Visual observation of the green output beam was taken as sufficient evidence of correct output wavelength. In addition, the North American high speed photodiode, provided as GFE, is designed to respond to a narrow wavelength range about the 1.06μm Nd:YAG fundamental wavelength, and did indicate the presence of the fundamental.

4.4.3 Test 7, 8 and 9, Power Stability and Pulse Duration

Average power and pulse duration, tests 7 and 9, were performed simultaneously. With a solar monitor reading of 6.75, 400 mW of mode locked, frequency doubled output was obtained with 280 psec duration pulses. The power was measured

Table 15

General Test Plan Tasks

Number	Test	Performed
1	Telescope Interface	X
2	Simulator Interface	X
3	OMS Interface	X(a)
4	Operation-Telescope	X
5	Operation-Simulator	X
6	Wavelength	X(b)
7	Average Power	X
8	Power Stability	X
9	Pulse Duration	X
10	Laser Rod Temperature	X
11	Polarization	X
12	TEM_{oo} Mode Locked Operation	X
13	Pulse Repetition Frequency	X
14	Clock Output Power	X
15	Clock Output VSWR	X
16	Clock Phase Stability	X
17	Clock Harmonic Content	X
18	Phase Ambiguity	X
19	Heat Sink Efficiency	No
20	Output Beam Wander	No (c)
21	Misaligned Operation	X
22	Pulse Duration/Power	X
23	Shock Vibration	No

(a) By comparison with drawing.
(b) Assumed
(c) Not required by Statement of Work

with CRL Model 212, Sylvania No. W150 power meter, calibrated against a meter which had just previously been calibrated at CRL. The pulse duration was inferred by taking twice the 1.06μm pulse rise time, divided by $\sqrt{2}$. The rise time was determined using the North American high speed photodiode to determine the 1.06μm rise time. The pulse duration at the 400 mW level was noted but not documented with a photograph. Such a photograph for operation with output power in excess of 300 mW is shown in Figure 22.

Average power stability test 8, was measured using the output of a CRL 212 power meter. The test was performed with the laser producing 310 mW of power with a solar monitor reading of 6.8, with pulse duration of 350 psec. The stability was measured using an oscilloscope for short term and a chart recorder for long term. Figure 23 (a), (b) shows photographs of the oscilloscope trace, 20 μsec/division and 2 msec/division horizontally, and 5 mV/division vertically on a dc level of 2.3 volts. The short term variation is 1.2 x 20 mV = .024 volts. This converts to $\pm$(.024/2.3/2) x 100% = $\pm$0.5%, well within the $\pm$2% specification. The chart recorder trace of Figure 23(c) shows a trace at 1"/minute for 6-1/2 minutes. The dip in power was caused by a high, wispy cloud passing between the sun and the telescope, the cloud taking about one minute to transit. After approximately 90 seconds, the laser had returned to pre-transient operation.

4.4.4 Test 10, Laser Rod Temperature

The laser rod temperature was monitored during all testing using the calibrated monitor unit. While often the temperature was between $0^{o}C$ and $-10^{o}C$, no difficulty was experienced in obtaining 350 mW of mode locked, frequency doubled output at $0^{o}C$ or slightly above, the $0^{o}C$ temperature being specified as the minimum laser rod operating temperature.

Table 16 presents laser output power and pulse duration as a function of rod temperature, which was controlled by maintaining the refrigerated coolant reservoir at appropriate temperatures by heating. During this test, the pulse duration was considerably greater than 300 psec, and could not be reduced while maintaining the average output power above 250 mW. Since the laser resonator was the same used for the previous tests, the difficulty was attributed to poor mode locking by the AOML/FD. This difficulty was encountered often during the testing.

Table 16

PSQM LASER PERFORMANCE vs ROD TEMPERATURE

Power (mW)	Pulse Duration (psec)	Rod Temperature (^{o}C)
341	620	1
329	560	6
282	560	11
256	560	13

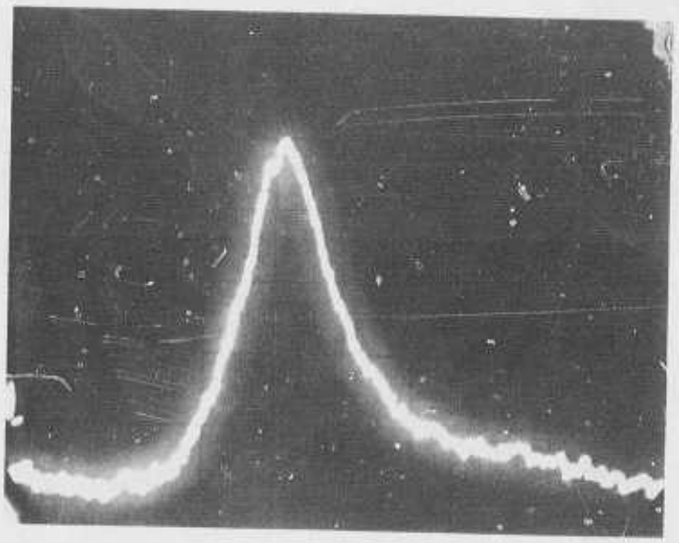

Figure 22 1.06μm Laser Pulse with 200 psec Rise Time (200 psec/division)

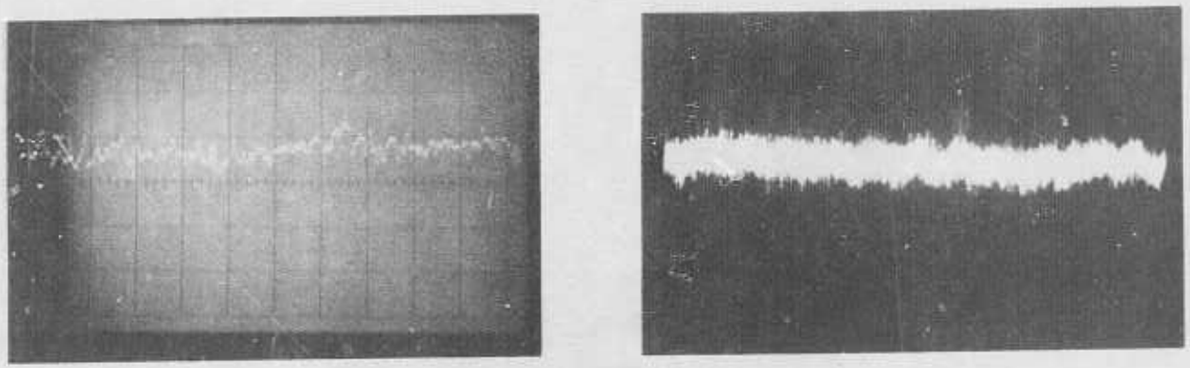

(a) (b)

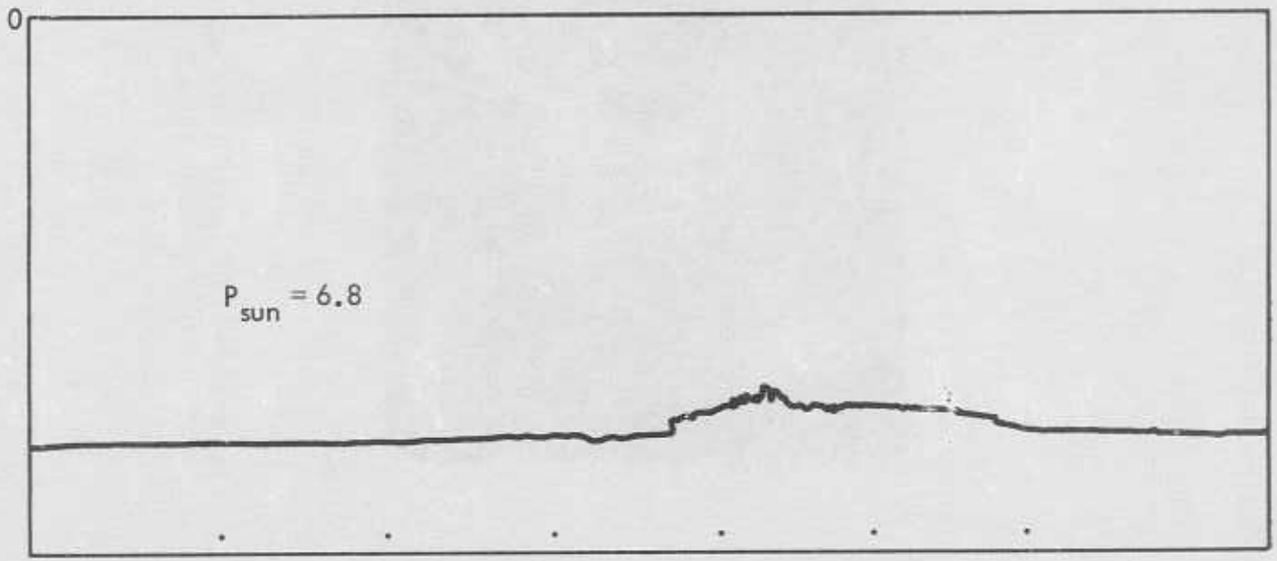

(c)

Figure 23 Average Power Stability of the PSQM Laser. (a) 20 μ sec/division, (b) 2 msec/division, (c) 1 minute/division

4.4.5 Tests 11, 12 and 13, Polarization, TEM_{00} Operation, and PRF

The laser rod temperature was monitored during all testing using the calibrated monitor unit. While often the temperature was between $0^{o}C$ and $-10^{o}C$, no difficulty was experienced in obtaining 350 mW of mode locked, frequency doubled output at $0^{o}C$ or slightly above. Variation of laser performance with rod temperature is discussed in Section 4.5.

For test 11, 0.53μm output beam polarization, a Glan-Thompson prism was used. The polarization ratio was 225:1. Because the laser mounting platform on the telescope moves during the day and is not horizontal, it was difficult to determine the polarization angle accurately. The direction was horizontal as desired with respect to the cavity L plane to within 2^{o}.

The mode structure of the laser output was observed for test 12 on a spectrum analyzer, and found to consist of a single transverse mode oscillating at 500 MHz. A transverse beam scan, shown in Figure 24, shows the beam to have a single maximum, typical of the TEM_{00} mode. The irregularities are attributed to etalon effects in the BSN crystal. The scan is in the horizontal plane (parallel to the cavity L). The laser was producing 360 mW with 500 psec pulses, with a solar monitor reading of 6.75.

The pulse repetition frequency was measured against a Hewlett-Packard 5245L counter. The prf was found to be within 20 kHz of the 500 MHz specification with a variation of less than 2 kHz for several minutes. The rate of change of prf was not measured.

4.4.6 Tests 14-18, Clock Detector Output

Test 14, measurement of the clock detector output power into a 50 ohm load, resulted in a power reading of -0.05 dBm, within the 0 dBm $\pm$1 dB specification.

Clock output VSWR, test 15, was measured to be 1.53 slightly in excess of the 1.5 specification.

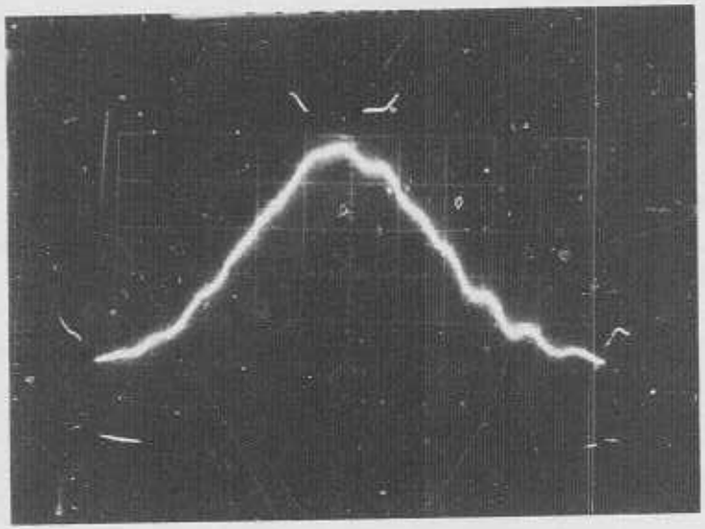

Figure 24 Laser Output Beam Scan

The clock phase stability, test number 16, was performed using a vector voltmeter to measure the phase variation between the clock output and the optical pulse train. The variation was less than $\pm 0.2^{o}$, well within the $\pm 4.5^{o}$ specification. The laser was producing 285 mW with 350 psec pulses, at a solar monitor reading of 6.7.

The clock harmonic content test number 17, was measured immediately after the above test. The results are summarized, in Table 17, and are acceptable.

Test number 18, for phase ambiguity, requires some explanation. In a previous lamp pumped laser program[4], phase state switching was observed. Such state switching is manifested by a shift in pulse position, as observed on an oscilloscope, by half the interpulse spacing. The AOML/FD drive was used as a reference signal. Since the state switching had been observed previously when two intracavity mode locking devices were used, none was expected with this laser.

Indeed, no phase ambiguity was noted during all the testing, and particularly during the five minute test.

4.4.7 Tests 21 and 22, Misaligned Operation and Pulse Duration vs Power

Laser performance was evaluated as a function of misalignment angle between the telescope output beam centerline and the laser input centerline. The laser mounting bracket allowed the laser to be pivoted about an axis through the cone lens, so displacement could be ignored. The results are shown in Figure 25. The laser was readjusted for maximum power and narrow pulsewidth for each position.

Next, a similar evaluation was performed with the variable being misalignment of the telescope with respect to the sun. This was controlled by stopping the clock drive for a short period to increase the misalignment by a known amount. The results are shown in Figure 26, and repeat fairly well similar results obtained on the previous program.[3]

Table 17

Clock Harmonic Content

Frequency Location	Power	Comment
250 MHz	-28 dBm	
500 MHz	0 dBm	Fundamental
750 MHz	-56 dBm	
1 GHz	-28 dBm	
1.5 GHz	-	Noise
Thermal	-65 dBm	
Random	-30 dBm	Unresolvable hash on 500 MHz signal

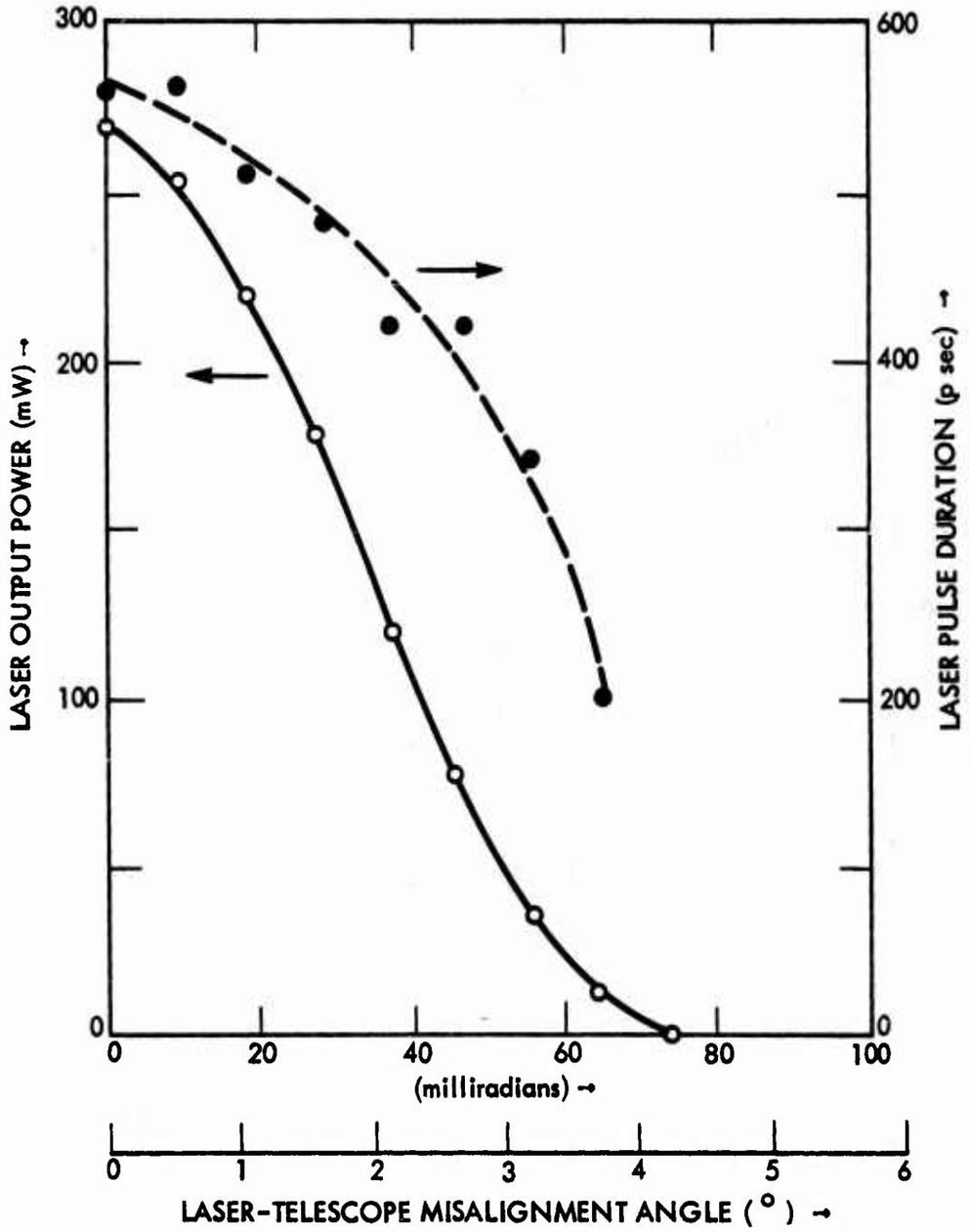

Figure 25 PSQM Laser Output Power and Pulse Duration vs Laser-Telescope Misalignment Angle

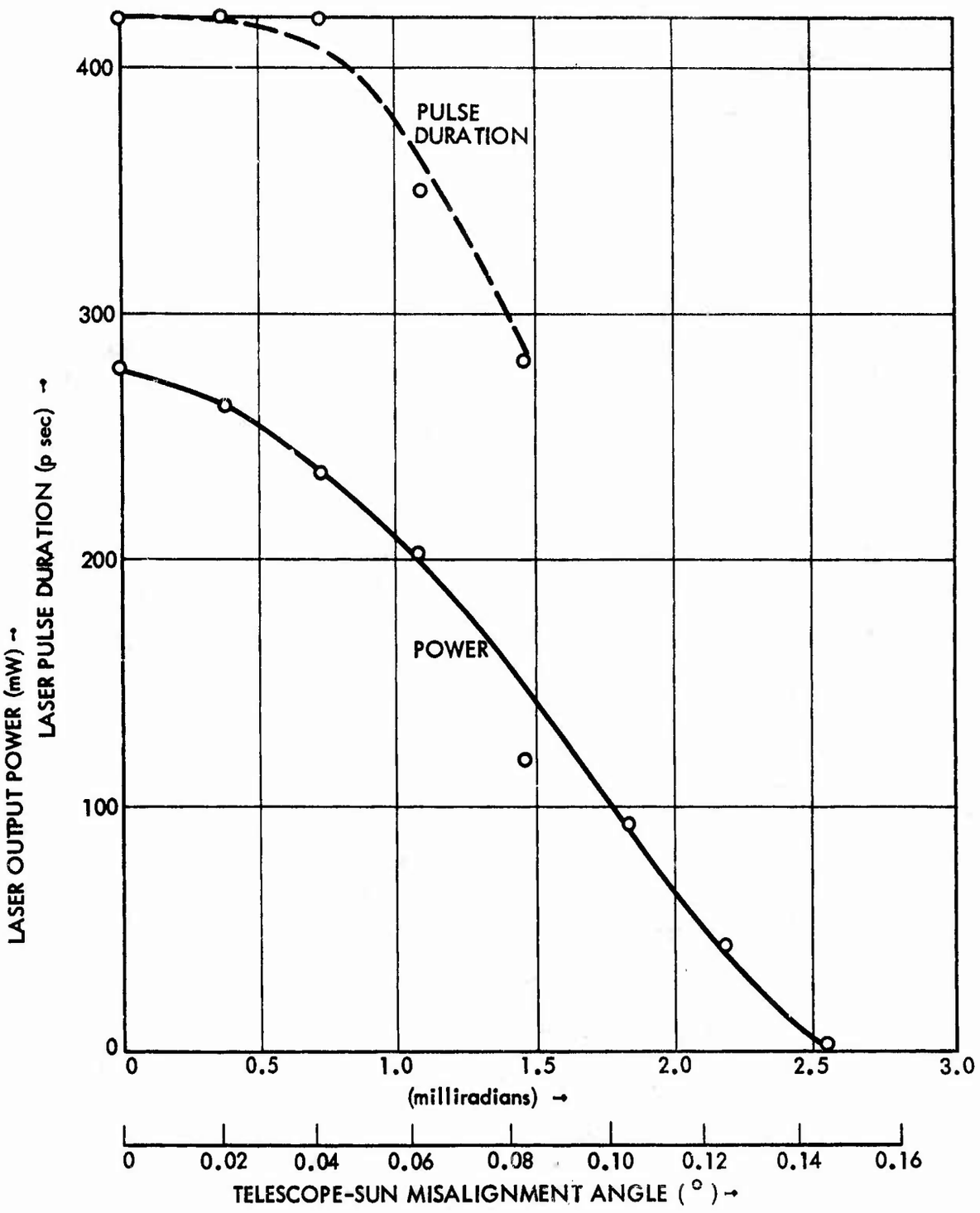

Figure 26 PSQM Laser Output Power and Pulse Duration vs Telescope-Sun Misalignment Angle

While data is herein presented from which pulse duration vs laser output power curves could be generated, the difficulty in maintaining short pulses during much of the testing would make such plots of questionable value. Representative data obtained by aperturing the telescope to vary power and pulse width is presented in Table 18 and shown graphically in Figure 27.

Finally, Table 19 presents multimode and modelocked, frequency doubled performance of Nd:Cr:YAG laser rod 107, solar pumped with several secondary mirrors.

Table 18

PSQM LASER PERFORMANCE vs TELESCOPE APERTURE

Aperture Ratio	Power (mW)	Pulse Duration (psec)	(^{o}C) Rod Temperature
.912	341	510	1
.830	341	560	0
.752	282	560	0
.637	227	480	-3
.539	142	280	-4
.440	107	280	-5
.353	43	210	-7
.252	9	120	-

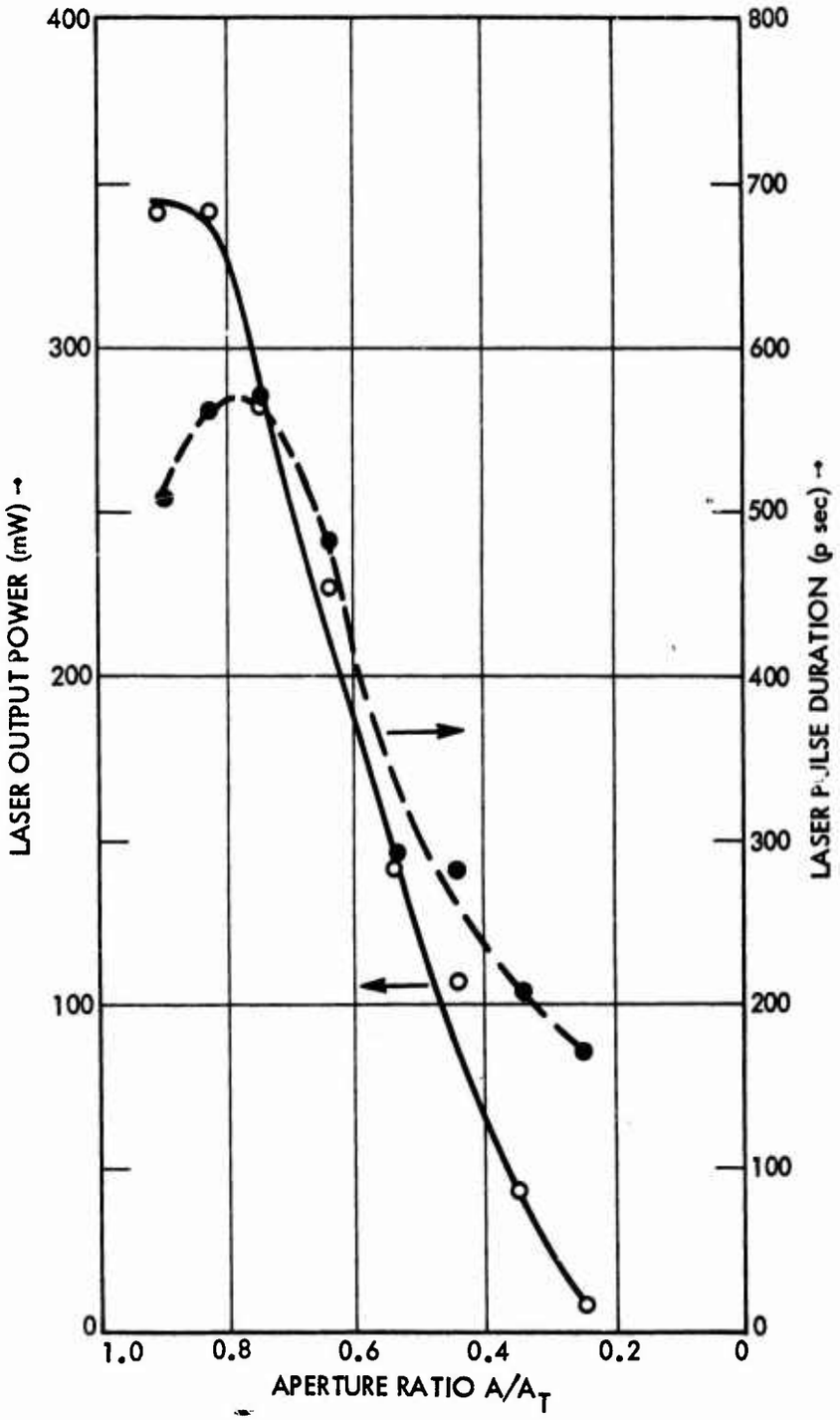

Figure 27 PSQM Laser Output Power and Pulse Duration vs Telescope Aperture

Table 19

SOLAR PUMPED PERFORMANCE OF LASER ROD 107

WITH SEVERAL SECONDARY MIRRORS

Mirror*	Multimode		Mode Locked/Frequency Doubled		
	Power (Watts)	Rod Temperature (^{o}C)	Power (Watts)	Pulse Duration (psec)	Rod Temperature (^{o}C)
2-1/2" silver	3.7	4	.17	280	-
3" dielectric wideband	4.0	-3	.34	280	-5
3" dielectric old narrowband	2.3	-5	.185	310	-7
3" dielectric new narrowband	2.1	-6	-	-	-

* See Table 11

4.4.8 Tests 19, 20, 23, Test Not Performed

Because contract funds were nearly expended, tests 19, 20 and 23 (heat sink efficiency, output beam wander, and shock and vibration respectively) were not performed. Test 19 would have required mounting of several heaters, extra thermocouples, careful calibration, and probably questionable interpretation of the data. Test 20 was not required by the contract statement of work, and was thought not to be a problem. Test 23 was performed successfully on the lamp pumped EFM laser, and the confidence generated by that led to a lowering of the priority for such testing on the PSQM solar pumped laser.

Available contract funds were used for conducting the laser performance tests.

Section V

OTHER TASKS

5.1 Protective Coatings for Reflective Surfaces in Space

5.1.1 Introduction

This summary contains information gained from a survey on protective coatings for reflective surfaces in space environments, specifically, information regarding the resistance of these coatings on both aluminum and silver surfaces to the destructive effects of hard ultraviolet radiation and ion bombardment from solar sources at intensities found in earth orbits.

The primary reflecting surface, to which one of the considered coatings will be applied, comprises the twenty-inch, parabolic collecting mirror of the sun pumped laser communications system. The surface will be required to last seven or more years without substantial degradation in reflectance.

In the following, sharp contrast is made between the use of silver and aluminum, since the physical properties of the two metals are well known. A preliminary contrast will also be made between the two categories of protective coatings, the flexible (polymers) and the non-flexible (oxides and silicates). Here, a direct comparison, as with the metals, cannot be made at this time for thin films under long term solar exposure conditions because published experimental data is not presently available.

An additional goal of this survey was to determine by whom and where research into coating survivability is presently being planned or conducted. A list of organizations capable of carrying out a responsible and accurate test program has been compiled and is included, should subsequent information on degradation effects be required.

5.1.2 The Behavior of Aluminum and Silver Surfaces

Reflectance of a material is a function of both angle of incidence and wavelength of incident light. It is also a function of polarization, but unimpeded

solar radiation is basically unpolarized. Surface irregularities and contaminants will affect the amount of light reflected, but these can be present in both types of metals and will be omitted at this point.

Assuming normal incidence, unprotected silver has the greater overall reflectance, ranging up to 98% for 0.55 μm and longer wavelengths. Near 0.45 μm its reflectance begins to drop noticeably, to a value of only 8% at 0.3 μm, then varying up and down more rapidly as the wavelengths become shorter, but rising to no more than an absolute 30% at these oscillatory peaks.

Unprotected aluminum averages about 91% from 0.2 μm to 0.75 μm in a very smooth manner, decreasing to 85% reflectance at 0.85 μm and again rising to a steady 93-94% beyond 0.95 μm.

(Thin film coatings applied to these bare metal surfaces, regardless of composition, will alter these behavior patterns somewhat.)

The spectral pumping region most critical to the operation of the sun-pumped YAG laser is from 0.5 to 1.0 μm. In this region, greatest reflectance is of utmost importance. From the properties of the metals discussed above, it is noted that this is where aluminum is least suitable. At 0.85 μm, near the center of the critical pumping region, its reflectance is an absolute 13% less than silver.

There is another advantage in using a silvered primary mirror rather than aluminum. In the cassegrain focusing system, the incident light is reflected backwards from the primary collector mirror onto a secondary mirror which then directs the light forward through a small aperture located on the axis of the primary. Because of the focusing method, the secondary surface would normally incur substantially higher amounts of UV radiation if the primary reflector were made of aluminum, for it reflects ultraviolet very well. Silver, on the other hand, has an enormous rise in the absorptance of these harmful wavelengths. At 0.35 μm, the reflectance begins to drop and at 0.3 μm it reflects only 8% of the incident radiation.

Even though the final product of absorption is heat, it is more easily dissipated at the primary, where energy concentration is only 1/60 that of the secondary. The elimination of most of the destructive ultraviolet light at the primary collector will greatly enhance the potential lifetime of the system.

5.1.3 Coatings

For these two metals, Al and Ag, protective first surfaces have been composed of the non-flexible MgF_2, SiO, SiO_2, Quartz, "FS-72" (a Denton Vacuum Inc. trade name, probably Fused Silica), unspecified "multi-layered dielectrics", and more recently the flexible polymer resins of teflon fluorocompounds.

While documented data relevant to silver and aluminum surfaces protected by hard or soft (polymer) films under long term solar irradiance is not yet available, limited comparisons can be made.

SiO_2 is probably the most inert in the non-flexible category under the prolonged effects of exposure to hard UV and ion bombardment. This information was gained at GE Space Division, and verbal estimates of degradation (in SiO_2) ran from a high of 2% per year drop in reflectance, to a low of 3.5% drop after ten years of continual exposure. (These figures were given by Mr. A. T. Tweedie and Mr. Al Liegles, respectively, at GE.)

Silicon dioxide's emissivity is also the highest of the hard films, allowing it to radiate the heat absorbed at lower temperatures. However, operating temperatures can be regulated by the substrate thickness as well as with the protective coating.

Another advantage of SiO_2 over the softer polymers is its increased resistance to damage by micrometeorite bombardment. The harder surface may only be "dimpled" in an area no larger than the particle diameter, whereas soft films may "gouge" deeper and wider than the incident particle dimensions. For applications of thermal control on the surface of spacecraft, this would be of extremely small concern, but as protection for an energy focusing surface, the added irregularities may cause a noticeable increase in random scattering and light absorption.

In current technology in teflon films, a protective layer is applied approximately 5 to 10 times thicker than the hard coats. Because teflon is fairly opaque in the visible spectrum, this added thickness will reduce some of the initial reflectance.

While knowledge of thin film behavior in space environments is virtually unknown, much testing has been done on block samples of TFE and FEP resins by DuPont De Nemours and Co. The information gained, as follows, will be able to answer a few questions on polymer behavior and also provide some insight as to why the end result of solar exposure in space is so hard to predict.

Relevant findings show that there is absolutely no danger of sublimation at vacuum pressures in the order of 10^{-7} mm Hg at 100°C. Theoretical calculations give a dissociation pressure of 5×10^{-12} mm Hg for the same temperature, this being lower than that for many common metals.

Changes in the physical properties due to irradiation are not easy to predict, and factors such as radiation dose, temperature during radiation, and pressure of oxygen (not applicable here) determine the type and amount of change. For instance, a structure whose parallel molecules have extended sideways and joined sideways movements of parallel molecules via radiation or other stimuli, are said to have "crosslinked". This crosslinking can sometimes be controlled to give harder, stronger material. If the molecular structure is broken into shorter molecules, a softer material with decreased strengths will result. Very high energy photons (x-rays, cosmic rays) will be more likely to break the chain; lower energy photons (ultraviolet) are more likely to knock them sideways. The final properties of the material are determined by the predominate action.

Teflon also tends to develop microcavities during processing, although this is not necessarily detrimental to the protective function and may be eliminated by vapor deposition. Additives dispersed in the teflon during the application to enhance certain properties have a tendency to diffuse out of the polymer at high temperatures and onto the underlying metal surface, which may change optical properties of the surface.

Thus, final judgement concerning the use of thin film teflon under long term exposures must be withheld until tests simulating the expected space environment have been concluded.

5.1.4 Testing

Thin film teflon coatings on silver and aluminum surfaces are only now being tested in large scale programs.

NASA-Langley has been monitoring two samples of "aluminized and silvered teflon" (teflon protected surfaces) on board an "earth orbiting platform" (designation unknown) for the past 9000 hours of flight time, 3200 hours of which have been in direct solar irradiance. The orbit of this vehicle ranges from 300 miles to 120,000 miles and passes through the Van Allen Belt. During the time of this surveillance, the silvered surface was found to increase in absorptance from .088 to .118 (a 3.4% loss in reflectance), while the aluminized teflon increased from .135 to .157 (a 2.6% loss in reflectance). The waveband over which these values were measured was not specified; neither was the type of detector. Obviously 3200 hours (.365 years) does not form an adequate basis for extrapolations to seven years, considering the above discussion of teflon, nor does the orbiting vehicle allow examination of the detectors themselves for radiation damage.

NASA is also conducting ground based simulations to determine photodegradation of aluminized and silvered teflon at the Boeing Corporation in Seattle. The actual test program was finished around January 1975, but the documented and printed results are not anticipated to be available until later in 1975.

SAMSO is conducting similar degradation tests on a wide variety of polymer coating films, many of which will not be applicable to the sun-pumped program, such as coated weaves to serve as canopy shields. SAMSO's tests are being done by TRW at Redondo Beach, California, under the direction of Mr. Richard Kirkland and results will not be published before July 1975. Sylvania has been placed on both mailing lists for complete and preliminary results as they are prepared.

General Electric Corporation has much information on hard surfaced protective films as well as their own testing facilities. The information on these films is classified, but can be obtained. Lockheed Corporation of Sunnyvale also has some pertinent data of the same nature which might be obtainable.

In a brief conversation with Mr. Al Liegles of GE Space Division, it was learned that more testing on SiO_2 and other hard overcoats under conditions of vacuum and simulated solar irradiance were being planned. Sylvania was offered concurrent participation in the program should it have additional samples to investigate.

Tables 20 and 21 list the known available testing facilities and the companies contacted for information.

5.2 Deformation Study of the Telescope Primary Mirror

An evaluation of the solar telescopes primary collector mirror was performed to establish a maximum allowable geometric figure error that could be present without significantly degrading the system performance. A target value was established which dictated that the total amount of solar energy vignetted by the optical collection and transfer train must not exceed 5%, excluding that of the central obscuration. This vignetting would be caused either by rays missing the specified clear apertures along the transit path to the YAG rod, or by retroreflection from the cone itself.

The analysis of the 24-inch, f/1.5 paraboloid was carried out using spot diagrams generated by PAGOS, the Aerospace Corporation's "Program for the Analysis of General Optical Systems". The mirror dish was subjected to both positive and negative deformation coefficients of fourth order in the aspheric expansion. This model was chosen as fabrication and mount induced stress errors tend to increase towards the edge of the mirror face. Figure 28 shows a typical fourth-order variation of deformation with (normalized) radius. This variation pattern, represented along the ordinate of the graph, was added to and subtracted from the basic second order parabolic shape.

Spot diagrams at on-axis and 1/4 degree off-axis field angles for primary mirror edge deformations up to 210λ were examined, where λ = 0.8 μm, the center of the main pump band. In terms of the other minor pump band lying between 550 and

Table 20

Organizations Having Facilities for Testing Coatings for Space

JPL, Pasadena, California

Person to see: Mr. Jim Noller (213) 354-3121

Description: Can handle samples with dimensions of 7' x 14" Vacuum test chamber with solar irradiances and ion bombardment simulators.

General Electric, Philadelphia, Pennsylvania

Person to see: Mr. Al Liegles (215)962-3974 or Mr. A. T. Tweedie (215) 962-3993

Description: At least as diverse (if not a larger size test chamber) as JPL.

TRW, Redondo Beach, California (testing now in progress)

Person to see: Mr. Dick Kirkland (213) 535-3557

Description: Unspecified.

Boeing, Seattle, Washington (testing now in progress)

Person to see: Mr. Wayne Slemp (804) 827-3041 - at NASA-Langley)

Description: Unspecified.

Martin Marietta, Denver, Colorado

Person to see: Mr. Robert Czarnecki

Description: Unspecified

Table 21

Companies and Organizations Contacted During the Protective Coatings for Reflective Surfaces in Space Effort

Evaporated Coatings, Inc.
Santa Rosa, California

Coherent Radiation
Palo Alto, California

Lockheed Research Labs.
Sunnyvale and Palo Alto, California

Broomer Research
Plainview, New York

Infra-Red Industries
Santa Barbara, California

Denton Vacuum
Cherry Hill, New Jersey

Aerospace Corporation
El Segundo, California

Hughes Aircraft Company
Culver City, California

Opticon Chemical Company
Palos Verdes, California

JPL
Pasadena, California

Ball Brothers
Boulder, Colorado

Air Force Materials Lab.
Wright-Patterson, Ohio

DuPont DeNemours
Los Angeles, California

Sadther Research Labs.
Philadelphia, Pennsylvania

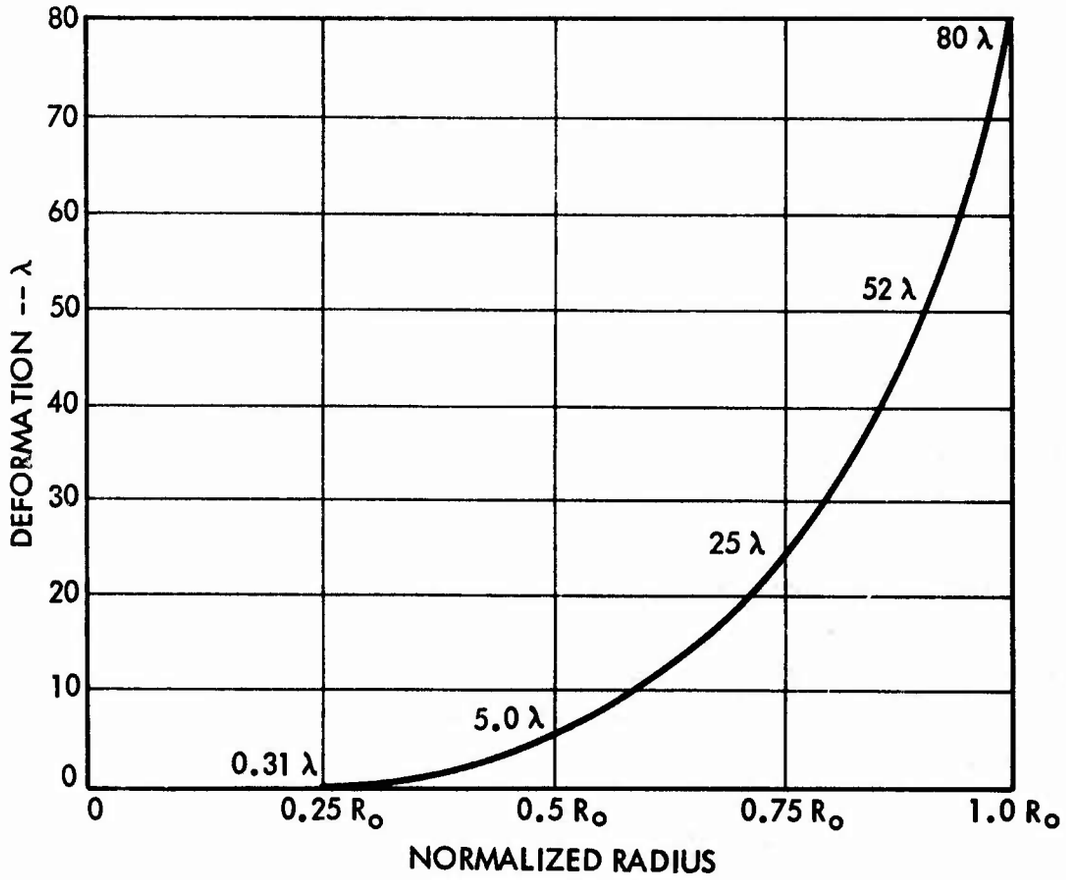

Figure 28 Typical Fourth Order Deformatory Behavior of the 24 Inch Diameter Solar Telescope Primary Mirror

650 nm, this deformation represents an approximate 280λ deviation from the parabolic shape.

As substantiated by the computer results, the geometric surface errors can be several orders of magnitude larger than would be required if the cassegrain configuration were being used for imaging. Spot diagrams from PAGOS revealed that vignetting from a positive fourth-order coefficient began to appear at 10 waves edge deformation, and increased linearly up to 120 waves where other effects began to occur. The negative coefficient effects appeared much later in the deformation process, with vignetting beginning at minus 60 waves, but increasing thereafter in a linear fashion as well. The behavior of both these processes is illustrated in Figure 29. The positive deformation tends to draw the parabola towards a spherical shape. (The parabola used in this particular instance represents a negative 232 wave error at the mirror edge from a spherical figure.) The negative coefficient tends toward the hyperbolic figure.

The positive coefficient appears to be the determining factor in setting basic minimum figure tolerances. A transferred loss of 5% total collected energy occurs with an edge deformation of 30λ, or 24 μm at λ = 0.8 μm. Present polishing processes exist that enable figure correction to fractions of a wave on well supported (rigid) polished surfaces. The positive 30, minus 60 wave figure error allowance suggests a small thickness to diameter ratio on the substrate.

5.3 Solid YAG Condensing Cone[9]

A theoretical evaluation of the effect on laser performance resulting from the use of a solid YAG condensing cone was made. The basic assumption was made that such a cone would allow all the light presently transferred to a 3 mm laser rod with the silvered air cone to be transferred to a 2 mm rod.

Considering single pass gain, internal loss and SHG loss of g_o, α_o, α_{SHG}, the second harmonic output power can be expressed [10] as:

$$P_{SHG} = \frac{2\,\alpha_{SHG}}{\beta} \left(\frac{g_o}{\alpha_o + \alpha_{SHG}} - 1 \right)$$

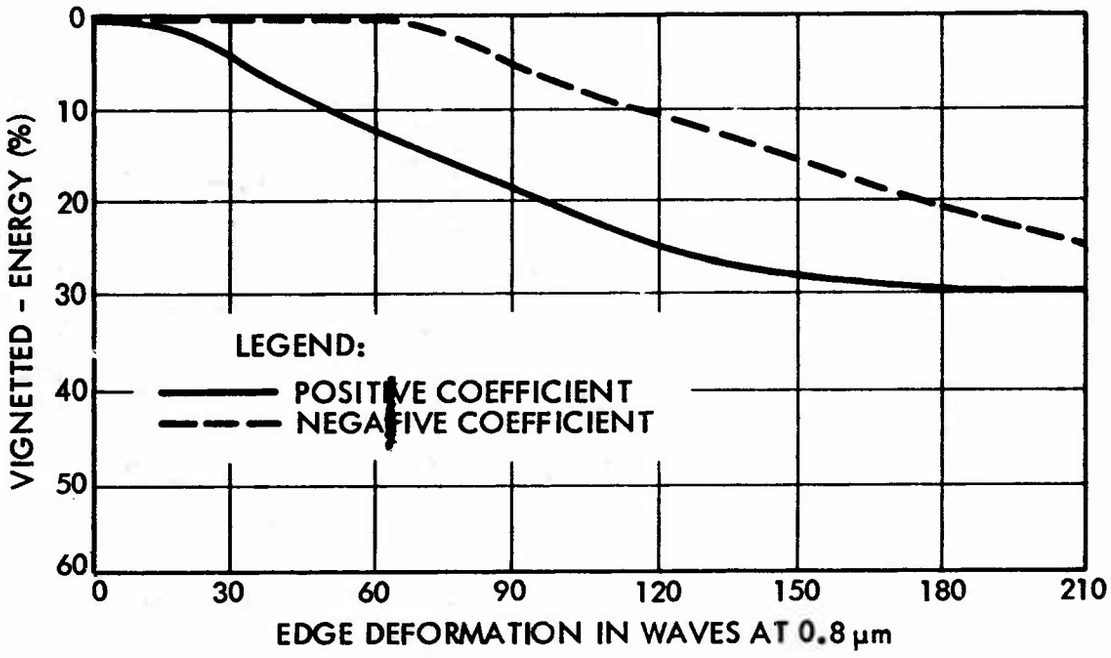

Figure 29 Vignetted Energy vs Edge Deformation for the Solar Telescope

where β is the saturation parameter. Maximizing P_{SHG} results in the following:

$$(P_{SHG})_{max} = \frac{2g_o}{\beta}\left(1 - \sqrt{\frac{\alpha_o}{g_o}}\right)^2$$

The following are definitions of g_o and β:

$$g_o = \frac{\eta P_p \tau\sigma}{Ah\nu_p} \qquad \beta = \frac{\tau\sigma}{Ah\nu_\ell}$$

where τ and σ are the upper laser level lifetime and absorption cross-section, $h\nu_p$ and $h\nu_\ell$ are the pump and laser photon energies, P_p is the pump power, η is the probability that an absorbed photon will excite an Nd ion, and A is the laser rod cross-sectional area. Thus, for the rest of the parameters held constant, g_o varies inversely with A. Assuming α_o is unaffected by rod diameter,

$$(P_{SHG})_{max} = 2\eta P_p \left(\frac{\nu_\ell}{\nu_p}\right)\left(1 - \frac{d}{3}\sqrt{\frac{\alpha_o}{g_o(3)}}\right)^2$$

where $g_o(3)$ is the gain for a 3 mm diameter rod, and d is the actual rod diameter in mm. Using the value of $g_o(3) = 0.052$ determined on the previous program,[3] and assuming several values for α_o, we can calculate the potential enhancement of the output power. This is summarized in Table 22. Thus, a substantial improvement can be obtained by using a smaller rod, provided all the pump power can be supplied to the rod.

Because of financial limitations imposed by other portions of the program being more costly than anticipated, the experimental portion of the solid cone study was not pursued. The approach appears promising, however.

Table 22

Potential Enhancement of Laser Output Power
Utilizing a Solid YAG Condensing Cone

g_o	α_o	P_{SHG} (2mm)/P_{SHG} (3mm)
.052	.0075	1.45
.052	.0100	1.59
.052	.0125	1.74
.052	.0150	1.92

The 2mm diameter rod can be used with a solid YAG cone.
The 3mm diameter rod can be used with an air cone.

5.4 Test Pump Cavities

One task on this program was to fabricate and deliver pump cavities and mounted laser rods for experiments at the laboratory at the Program Office. Because of changes during the EFM lamp pumped laser program, two configurations including two rod sizes were delivered.

The first configuration was virtually identical to that used in the lamp pumped Brassboard Laser Transmitter, employing a 3mm x 54.5mm laser rod. The second was a prototype of the final version of the actual EFM laser pump cavity. Three of each configuration were fabricated and delivered. In addition, a seventh laser rod was mounted on a separate heat sink, both items compatible with the EFM design.

All pump cavities employed dielectric coated pyrex inserts for pump source filtering, conductive cooling of the cavity block and laser rod, and flowing refrigerated liquid cooling of the cold plate.

Section VI

SUMMARY AND CONCLUSIONS

During this program, a PSQM solar pumped laser was designed, fabricated, assembled and tested. An extensive development effort was undertaken during the early part of the program to facilitate mechanical design. This effort extended through most of the program to aide in optimization of the PSQM laser.

Laser rod bonding was investigated, resulting in a better understanding of the bonding requirements and in an improved procedure for bonding the rod in its heat sink. The dependence of laser output power as a function of forced polarization was investigated as part of the bonding development. Laser rods bonded with the developed procedure produce maximum power for the desired vertical polarization.

Based on tests with available laser rods, 1% Nd and 0.1% Cr doping of YAG was chosen as optimal, and produced the highest output powers observed in all cases: multimode and TEM_{oo} mode, polarized and unpolarized, solar simulator pumped and solar telescope pumped, and with all available secondary mirrors. Because the laser rods procured on this program were inferior to the best rods available from previous programs, it is concluded that careful rod selection is needed for maximizing power output for future lasers.

The basic laser resonator was analyzed based on modelling performed on the EFM lamp pumped laser program.[5] The result was a set of candidate resonator cavities, the variables being dichroic mirror radius of curvature, intracavity lens focal length and intracavity lens position. A number of the most promising resonators were evaluated by operating them at 1.06μm and 0.53μm, cw and modelocked. Developmental testing utilized the solar simulator and the demonstration laser from the previous program[3]. PSQM laser optimization was carried out with solar telescope pumping.

The PSQM laser incorporated much EFM lamp pumped laser design, the differences resulting primarily from the end pumping geometry used with solar pumping.

The condensing cone, the final element in the optical pumping train, was replicated rather than electroformed. A light trap was used to collect most of the unabsorbed pump source light exiting the laser rod. A large adjustable mount was used to hold the cone lens/HR 1.06μm mirror combination. One cold plate was used to cool the three primary heat producing elements: the condensing cone, the laser rod heat sink, and the light trap. The dichroic mirror mount, intracavity lens mount, folding mirror assembly, AOML/FD mount, and clock detector assembly are virtually identical to their EFM lamp pumped laser counterparts. The invar laser structure also is very similar, except for the laser rod and pumping section.

The laser operated stably mode locked, frequency doubled, and polarized. With a Nd:Cr:YAG laser rod, 400 mW output with 280 ps pulse duration was obtained. The germanium clock detector performed well, and requires less amplification than does the silicon device used in the EFM lamp pumped laser. Average power stability was limited by the stability of the pump light provided by the solar collecting telescope.

For the future, several areas should be addressed to modify the design prior to the proposed satellite experiment. Actual exospheric solar spectral measurements are needed to determine pump light power levels, level of ultraviolet which must be withstood by exposed components, and variation expected with time and with position of the earth in its orbit. A solar collection system must be designed which provides pump light stably with time, to minimize laser output fluctuations. Life testing of optical components must be performed. A laser rod selection program is needed to choose the best rod for the flight laser.

While further work is needed, the laser developed on this program has advanced the state of the art from laboratory demonstration level to engineering feasibility demonstration level, equivalent to that of the present engineering feasibility model lamp pumped laser. The solar pumped laser has been demonstrated to be suitable for efficient operation in the proposed space data relay system.

REFERENCES

1. L. Huff, "Sun Pumped Laser," Final Technical Report AFAL-TR-71-315, September 1971, AF Contract No. F33615-74-C-1255.
2. L. Huff, "Sun Pumped Laser," Final Technical Report AFAL-TR-72-310, November 1972, AF Contract No. F33615-72-C-1240.
3. L. Huff, "Sun Pumped Laser," Final Technical Report AFAL-TR-73-368, October 1973, AF Contract No. F33615-73-C-1142.
4. R. S. Reynolds, "Brassboard Laser Transmitter," Final Technical Report AFAL-TR-73-339, December 1973, AF Contract No. F33615-73-C-1140.
5. M. Ross, "Engineering Feasibility Model Laser Transmitter," draft of Final Technical Report submitted on AF Contract No. F33615-74-C-1028.
6. Dr. Richard Smith, National Bureau of Standards, private communication.
7. H. Kogelnik and T. Li, "Laser Beams and Resonators," Applied Optics, Vol. 5, No. 10, p. 1550, 1966.
8. L. Huff, J. D. Taynai, G. A. Massey, "Space Laser Design," Final Technical Report AFAL-TR-72-412, November 1972, AF Contract No. F33615-72-C-1629.
9. Dr. A. E. Siegman, Stanford University, private communication.
10. J. D. Foster and R. F. Kirk, "Space Qualified Nd:YAG Laser," Final Technical Report NASA CR-1771, October 1971.

☆ U. S. GOVERNMENT PRINTING OFFICE: 1976 — 657-630/1086